Underpinning wheat physiological and molecular responses to co-occurring iron and phosphate deficiency stress

Gazaldeep Kaur[1,2*], Vishnu Shukla[1*], Varsha Meena[1], Anil Kumar[1,2], Jagtar Singh[2], Pramod Kaitheri Kandoth[1], Shrikant Mantri[1], Hatem Raouched[3,4,5], and Ajay Kumar Pandey[1#]

Author affiliations

[1]National Agri-Food Biotechnology Institute (Department of Biotechnology), Sector 81, Knowledge City, Mohali-140306, Punjab, India.

[2] Department of Biotechnology, Panjab University, Punjab, India.

[3]BPMP, Université de Montpellier, INRA, CNRS, Montpellier SupAgro, 34060 Montpellier, France.

[4]Department of Plant, Soil, and Microbial Sciences, Michigan State University, East Lansing, MI 48824

[5]Plant Resilience Institute, Michigan State University, East Lansing, MI 48824

[*]Both the authors contributed equally

[#]*Corresponding author*

Dr. Ajay K Pandey, Scientist-E.

National Agri-Food Biotechnology Institute (Department of Biotechnology), Sector 81, Knowledge City, Mohali-140306, Punjab, India.

Telephone: +91-1724990124

Email: pandeyak@nabi.res.in; pandeyak1974@gmail.com

ORCID iD: https://orcid.org/0000-0003-1064-139X

ABSTRACT

Iron (Fe) and phosphate (P) are essential mineral nutrients for plant growth and development. While it is known that Fe and P pathways interacts within plants however, our understanding of the molecular mechanisms regulating nutrient interaction during plant vegetative and reproductive stages remains largely unknown. Herein, we provide a comprehensive physiological and molecular analysis of hexaploid wheat response to single P/Fe and combined Fe and P deficiency. Our data showed that wheat primary root growth was inhibited in response to –Fe, and remarkably rescued by co-occurring deficiencies of Fe and P. Transcriptome analysis revealed drastic and distinct molecular rearrangements to adapt the single and combined nutrient stress with dominance of Fe responsive cis-regulatory elements. Gene-based clustering and root-specific transcriptome expression analysis identify several important unique components induced in response to combined stress –Fe–P, including UDP-glycosyltransferases and cytochrome-P450 and glutathione metabolism. These data are consistent with our metabolome data, which further reveals specific metabolite accumulation in –Fe–P those include amino-isobutyric acid, arabinonic acid and aconitic acid. Finally, at reproductive stage alleviations of the negative effect of Fe was also observed in –Fe–P (i.e. spikelet development). Collectively, the data obtained is essential for designing new strategies to improve resilience of crops to cope with the limited nutrients in soils.

Keywords: iron, phosphate, *Triticum aestivum*, nutrient homeostasis, growth, transcriptome.

Highlight: Hexaploid wheat showed distinct physiological and molecular changes during single and combined deficiency of iron and phosphate. Alleviations of the negative effect of -Fe was observed in –Fe–P combined deficiency in the root phenotype and spike development.

INTRODUCTION

Nutrient deficiencies in plants severely reduce the crop yields and subsequently affect the worldwide nutrient balance (Marschner, 1995). Fe is an essential microelement for plant growth and development, utilized in nearly every cellular process ranging from photosynthesis to respiration. In general, deficiency of iron (Fe), especially in alkaline calcareous soil considered as one of the most critical limitations in cereal crop production (Ma and Ling, 2009; Abadia *et al.*, 2011). The rhizospheric region of the plants, including its composition, pH and oxidation state influences the Fe availability and its uptake mechanism by the roots (Morrissey and Guerinot, 2009) . To overcome Fe-deficiency, plants have evolved tightly controlled adaptive mechanisms, which involves the developmental response of root system to maximize Fe acquisition from the soil. Plants recruit two modes of strategies to transport Fe, strategy I, which is a reduction-based strategy found in non-graminaceous plants and strategy II which is chelation-based strategy found in graminaceous species. Strategy I, involves the lowering of the pH of the rhizosphere via excretion of protons, resulting in reduction of ferric chelate of the root surface and absorption of ferrous ions across the root plasma membrane (Kobayashi and Nishizawa, 2012). Ferric (Fe^{3+}) is the major abundant form in rhizosphere, which is the insoluble form of iron and cannot be taken up by the plants. In contrast during the strategy II, the uptake of Fe relies mainly on the biosynthesis and secretion of phytosiderophores (PS), such as mugineic acids (MAs). These biochemicals make Fe-PS complexes that are subsequently transported into the roots by yellow stripe like transporter proteins (YSL) (Curie *et al.*, 2001; Murata *et al.*, 2006; Inoue *et al.*, 2009; Lee *et al.*, 2009; Nozoye *et al.*, 2011; Kobayashi and Nishizawa, 2012). The molecular players involved in efflux of MA are now characterized in rice barley and very recently identified in wheat (Nozoye *et al.*, 2011; Kaur *et al.*, 2019).This raises the question about the extent to which the regulation of Fe homeostasis in monocots (cereals) depends on the availability of other nutrients.

Phosphorus (P) is an essential macronutrient for plants to complete their life cycle, and its deficiency is a major limiting factor in the crop productivity (Raghothama, 1999; Heuer *et al.*, 2017; Carstensen *et al.*, 2018). Different crops recruit adaptive physiological and molecular changes to acclimatize to P-deficiency (Rouached *et al.*, 2010; Secco *et al.*, 2017). The P-deficiency response results in multiple root developmental changes to enhance its acquisition along with the changed expression profiles of important genes involved in Pi

transport and distribution (Misson *et al.*, 2005; Bouain *et al.*, 2016). Based on the functional characterization in model plant *Arabidopsis* (dicots) and in rice (monocots), key players known to be involved in P starvation are transcription factor PHOSPHATE STARVATION RESPONSE (*PHR1*), microRNA399 (miR399), PHOSPHATE1 (*PHO1*) and ubiquitin E2 conjugase (*PHO2*) (Cai *et al.*, 2012; Oono *et al.*, 2013; Secco *et al.*, 2013). Root architecture changes are also reported in response to Pi deficiency (Svistoonoff *et al.*, 2007). For instance, in *Arabidopsis* the elongation of the primary root is inhibited under low P (Ward *et al.*, 2008*b*). Key genes involved in this process were discovered including *LPR1 (*LOW PHOSPHATE RESPONSE 1) (), *LPR2*, and PHOSPHATE DEFICIENCY RESPONSE 2 (*PDR2*) those are involved in local Pi sensing at the root tip level (Naumann *et al.*, 2019). Roots tips are an active site for Pi sensing that is shown to be mediated by SENSITIVE TO PROTON RHIZOTOXICITY (*STOP1*) and ALUMINUM ACTIVATED MALATE TRANSPORTER 1 (*ALMT1*) resulting in the accumulation of the apoplastic Fe mediated by malate (Mora-Macías *et al.*, 2017; Zhou *et al.*, 2020). This suggests that to cope the nutrient stress, roots also undergo metabolic reprogramming.

Besides *Arabidopsis*, most of monocot plants including maize, rice and wheat showed no reduction or slight elongation of primary roots under P-deficiency (Narayanan, A. Reddy, 1982; Mollier and Pellerin, 1999; Shimizu *et al.*, 2004).While in *Arabidopsis* the primary root inhibition was proposed to be partly due to Fe toxicity at root tip (Ward *et al.*, 2008*b*), no Fe toxicity is reported in cereal crops grown under P deficient condition. Thus the overall performance of the plants depends on the Pi availability and its interaction in the complex rhizospheric area with Fe and other metals (Bouain *et al.*, 2014; Xie *et al.*, 2019). So how monocots (cereals) coordinate P and Fe remains largely unknown.

Given to their opposite charge, Fe (II) is known to readily interact with inorganic phosphate (HPO_3-, Pi) in the soil or growth medium, near root surface and within the plant. When both Pi and Fe are absorbed at the same time, availability of both the nutrients gets affected due to precipitation (Dalton *et al.*, 1983). Multiple studies have provided the preliminary clue for the probable interaction of P with the absorption of important micronutrients like iron (Fe) (Chutia *et al.*, 2019; Xie *et al.*, 2019). It has been reported that under P-deficiency, reduced expression of Fe homeostasis related genes could be due to enhanced Fe availability to the roots under low P (Hirsch *et al.*, 2006; Ward *et al.*, 2008*b*). Although, downregulation of Fe-homeostasis specific genes was observed during P-

deficiency, the physiological and molecular effects during combinatorial lowering of P and Fe remain obscure.

Wheat is an important crop and is the major source of nutrition. Studying the molecular attributes of Fe and P crosstalk will help in designing a suitable model to optimize crop productivity during nutrient deficiency. Nevertheless, to date, despite its primary interest, a molecular event recruited by wheat to cope with P and Fe combined stress still waits examination. In the current study we performed a comprehensive analysis of physiological, transcriptional and metabolic changes in hexaploid wheat under single –Fe and –P and combinatorial deficiencies of Fe and P (–Fe–P). Special focus was laid to dissect the underlying molecular events in crosstalk of Fe and Pi during plant growth till their spike production, by combining transcriptomic and metabolomic approaches. An important role of genes involved in strategy II mode of Fe uptake under contrasting regimes of P was observed. Distinct transcriptional and metabolic regulation was observed in the roots of wheat during –Fe–Pi response. Knowledge gained in this study expands our understanding of how cereal crops respond to multiple simultaneous nutrient stress and how those are coordinated at the whole plant level.

MATERIALS AND METHODS

Plant materials

A bread wheat variety ‘C-306’ was adopted and grown hydroponically under the Hogland’s nutrient solution containing (L^{-1}): 6 mM KNO_3, 1mM $MgSO_4.7H_2O$, 2 mM $Ca(NO_3).4H_2O$, 200 µM KH_2PO_4, 20 µM Fe (III) EDTA, 0.25 mM H_3BO_3, 0.002 mM $MnSO_4.H_20$, 0.002 mM $ZnSO_4.7H_20$, 0.0005 mM $CuSO_4.5H_20$, 0.0005 mM $Na_2.MoO_4$ and 0.05 mM KCL. After overnight stratification at 4°C, wheat seeds were germinated for 5 days in distilled water. Once the endosperm starts browning it is removed from the developing seedlings. Seedlings were then transferred to PhytaBox™ and grown in the nutrient solution described above. After 7 days, nutrient solutions were replaced on the basis of different treatments. For +Fe–P treatment, 20 µM KH_2PO_4 was used for P-deficiency. For –Fe+P treatment, 2 µM Fe (III) EDTA was used for Fe-deficiency. While for –Fe–P treatment, 20 µM $KH_2PO_4$and 2 µM Fe (III) EDTA was used for both Fe/P deficiency. For control plants (+Fe+P) concentrations of nutrients were unchanged in above mentioned Hoagland’s solution. After germination, plants were grown in the described medium for 20 days in growth chamber set at 20 ± 1 °C, 50–70% relative humidity and photon rate of 300 µmol quanta m^{-2} s^{-1} with

16 h day/8 h night cycle. The whole set of experiment was repeated four times to examine biological variation. For sampling, roots and shoots were collected at different time points after deficiency (5d, 10d, 15d and 20d). Samples were snap frozen in liquid nitrogen and stored at -80°C. On the basis of distinct phenotype samples collected at 20 days after deficiency (DAT) were used for further analysis. To distinctively observe primary root and 1st order lateral root, individual plants were moved onto a 150mm wide petriplate filled with distilled water and characteristics was manually examined. Eight biologicals replicated for each above-mentioned treatment were used to ascertain root characteristics.

For the prolonged iron and phosphate deficiency individual seedlings were transferred into respective pots filled with soilrite (5 seedlings each) in three replicates manner and allowed to grow in growth chamber set at 20 ± 1 ºC, 50-70% relative humidity and photon rate of 300µmol photons m^{-2} with 16h day/8h night cycle. Pots were watered with Hogland medium solution with the condition as mentioned above twice a week. The main individual spikes of the each replicate were tagged at the first day after anthesis (DAA). Total of 15 plants were sampled for each condition. After the maturation of the plants (55 days), spike tissues (rachis, glumes and awn) were harvested and images were processed. For comparing morphological differences and length of matured spike from each condition was measured.

RNASeq experiment design and sequencing

Wheat 20 days old root tissue samples for the four conditions (+Fe+P, +Fe–P, –Fe+P and –Fe–P) with at least two to three biological replicates derived from at least two independent RNA extractions were pooled together. Each of biological replicates consists of 12-15 seedlings per treatment. Samples were collected at the same time, snap frozen in liquid nitrogen and stored at -80°C. The RNA extraction as well as Illumina sequencing was performed for two biological replicates for –P and three for –Fe–P with their respective controls. For Fe-deficiency. previously published RNAseq datasets were used (Kaur *et al.*, 2019). RNA extraction for library construction from the control and treated root samples was performed as reported earlier (Kaur *et al.*, 2019). Briefly, sequence libraries were prepared from high quality, quality control passed RNA samples using Illumina TruSeq mRNA library prep kit as per the instructions (Illumina Inc., USA). The reads were sequenced using 2 X 150 bp chemistry on NextSeq 500 and NovaSeq6000.

Sample clustering and differential expression analysis

Paired-end reads were quality trimmed and adapter filtered using Trimmomatic v0.35 to retain only good quality reads (QV>20). The clean raw reads were quantified for expression by pseudoalignment against wheat transcriptome (ensembl release 46) using Kallisto v0.44.0 (Bray et al., 2016), using the option --rf-stranded for stranded samples. DESeq2 R package (Love *et al.*, 2014) was used for differential expression analysis. Raw counts values from Kallisto were summarized from transcript to gene level abundances and imported for use with DESeq2 using tximport package (Soneson *et al.*, 2015). Principal Component analysis (PCA) was performed based on VST transformed counts for all samples to observe clustering across replicates and conditions. The samples from batches were taken together to build a DESeq2 model to obtain normalised counts, which were transformed using VST mode and corrected for the associated batch effect using remove Batch Effect function from limma package (Ritchie *et al.*, 2015). ggplot2 package (Wickham, 2017) was used to design the PCA plot. Clustered heatmap for selected 500 genes with highest variation in expression among the conditions was generated using pheatmap package.

For differential expression analysis, DESeq() function was used to calculate the relative expression for the pairwise comparisons among conditions. Log2 Fold Changes (LFC) were obtained for the pairwise comparisons for each of the three deficiency conditions w.r.t. control (+Fe+P) from the respective batch group only, so as to avoid any variation due to batch effects. The relative expression ratios were shrunk using apeglm package (Zhu *et al.*, 2018) to adjust the LFC of genes with extremely low counts.

Functional enrichment analysis and annotation

KOBAS (KEGG Orthology-Based Annotation System) standalone tool was used to firstly annotate wheat genes based on blast mapping against rice RefSeq and RAP-DB sequences, e-value $<10^{-5}$. For pathway enrichment analysis, identify module was used to shortlist the significantly overrepresented KEGG pathways for the respective deficiency conditions using Fisher's exact test. FDR correction was performed using Benjamini and Hochberg method. Also, MapMan (Thimm et al., 2004) was used to map the DEGs onto metabolic, regulatory and other biological categorical pathways. The mapping file was generated through Mercator (Lohse et al., 2013), using the wheat transcriptome fasta file as an input. In addition, wheat RefSeq v1.1 annotation released by International Wheat Genome Sequencing Consortium (IWGSC) was also used (https://urgi.versailles.inra.fr/download/iwgsc).

Identification of cis-regulatory elements

To check the extent of Fe or P specific transcriptional regulation in –Fe, –P as well as combined deficiency of –Fe–P, 2000 bp upstream promoter region sequences for the three sets of DEGs were downloaded from Ensembl Biomart. The promoter sequences were checked for presence of 115 frequent cis-regulatory elements (freq-CREs) enriched in clusters for gold standard (GS) Fe responsive genes (Schwarz et al., 2020) and phosphate regulation specific CREs using an in-house perl script (link). For validation and comparison, three sets of control groups with 100 promoters each were randomly shortlisted from genes that were not altered in response to Fe-deficiency (-0.5 > LFC < -0.5).

Gas chromatography–mass spectrometry metabolite profiling

Extraction of total metabolites was performed similarly as previously described (Wang et al., 2018; Kaur et al., 2019). Wheat roots subjected to +Fe+P, +Fe–P, –P +Fe and –Fe–P were sampled at 20 days after deficiency in triplicate manner and processed for metabolite extraction. The derivatized metabolites were analysed with a GC instrument (Agilent technologies 7890, USA) coupled with mass spectrometry. Measurement from an injection volume of 1 µl was taken in split-less mode in DB-5 column (30 m × 0.25 mm, 0.25 µm film thickness, Agilent) using helium as carrier gas. For analysis, qualitative analysis of chromatograms was performed in MassHunter Qualitative analysis Sp1 workstation (Agilent, USA). Identification and annotation of each compound was supervised manually using AMDIS software and NIST08 database (http://www.nist.gov/srd/mslist.html). Data were normalized to sample weight and internal control (sorbitol). Statistical analysis was performed as described earlier (Quanbeck *et al.*, 2012). Log2 ratio of metabolite abundances in tested conditions was plotted against control condition (+Fe +P). Delta method approximation was used to calculate standard errors (se) of log-ratio, se log-ratio = 1/ln $2\sqrt{[(SE_T/T)^2 + (SE_C/C)^2]}$, where SE_T and SE_C are standard errors of average test and control metabolite abundances. For PCA and hierarchical clustering analysis, clustvis (https://biit.cs.ut.ee/clustvis/) online program package with Euclidean distance as the similarity measure and hierarchical clustering with complete linkage was used. A tab-delimited file was used as input comprising of annotated metabolites with their corresponding log transformed concentration values in triplicates for each condition.

Quantitative real time-PCR (qPCR) analysis

Total RNA was isolated from the roots of the 20 DAT (days after treatment) seedlings. A total of 2ug of RNA was used to prepare cDNA by using SuperScript III First-Strand Synthesis System (Invitrogen, USA). For removing the genomic contamination in the RNA sample, they were pre-treated with TURBO DNA-free kit (Ambion, TX, USA). To perform quantitative RT- PCR **(**qRT-PCR) amplification was performed using gene specific primers (Table S1) along with internal control ARF (ADP-Ribosylation Factor) to normalize the expression data for each gene by the using of Ct method [$2^{(-\Delta\Delta Ct)}$] in the CFX96^{TM} Real-Time PCR System (BioRad Inc, USA). Two or three independent replicates with four technical replicates were performed for each sample. The relative amount of gene expression was calculated by $2^{-\Delta\Delta CT}$ method (Livak and Schmittgen, 2001) for every cDNA samples.

Metal analysis in wheat tissues, Perl staining and root Fe mobilization assay

Seed phosphorus and different metal analysis was performed using Inductive Coupled Plasma-MS (ICP-MS). Metal analysis was performed as described previously (Bhati *et al.*, 2016; Aggarwal *et al.*, 2018). Briefly, the mature seeds were grounded to fine powder and subsequently subjected to the microwave-digested with HNO_3 (SuraPure^{TM}, Merck). Respective metal standards were also prepared for analysis. Three independent replicates were performed for each 20 DAT samples. For Perl staining, wheat roots were incubated with Perl's Prussian blue (PPB) method consisting of with equal amount of premixed solution of 4% (v/v) HCL and 4% (w/v) Potassium hexacyanoferrate (II) trihydrate. Roots of eight to ten wheat seedlings from each experiment were taken and incubated in above solution mixture for 30 mins. Blue colour Fe-plaques were observed for the presence of Fe on the wheat roots seedlings and representative images (five seedlings per treatments) were taken for respective treatments. To estimate the PS release, Fe remobilization assays of wheat roots was performed in aerobic condition as described earlier in detail (Takagi, 1976; Kaur *et al.*, 2019). For PS release twenty-five wheat seedlings undergoing the respective treatments were used for release in 60 ml deionised water in presence of Micropur (Katadyn, Switzerland). The final concentration of the released ferrous ion was estimated by measuring OD at 562 nm.

Statistical data analysis and data availability

To identify significant differentially expressed genes, a cut-off criterion of LFC > 1 in either direction, with an adjusted p-value (padj) of less than 0.05 was set. The padj values were obtained by using the Benjamini and Hochberg approach for controlling the false discovery

rate. The RNAseq data generated in this study has been deposited under the NCBI SRA database BioProjectID (submission pending).

RESULTS

Fe and P interplay to regulates Fe uptake.

Wheat responses to either Fe or P deficiency are fairly documented at physiological and molecular level (Oono *et al.*, 2013; Kaur *et al.*, 2019). But little information is available on how wheat integrates simultaneous Fe and P stress and how wheat adjusts it growth capacity accordingly. Therefore, we compared wheat growth under four growth conditions, namely nutrient-sufficient (+Fe+P), single nutrient deficiency (–Fe+P, +Fe–P), and combined nutrient deficiency (–Fe–P). Short (5 days post treatment, dpt), medium (10 dpt) and long-term (20 dpt) effects of these nutritional growth conditions on wheat morphology and biomass allocation pattern were assessed. At all the time points, Fe-deficient plants displayed shorter roots compared not only to control (+Fe+P) plants but also to plants grown on –P and –Fe–P conditions (Figure 1A & B). The primary root length significantly increased during –P condition. Interestingly, combined Fe and P (–Fe–P) lead to the recovery of total primary root elongation, thus alleviating the negative effect of Fe-deficiency (Figure 1C). Similar trend was also observed for the number and length of the 1st order lateral roots which shows significant increase during –P and –Fe–P conditions compared to just Fe-deficient and control plants (Figure 1D and E). Examination of the fresh biomass allocation patterns from shoot to root was assessed as well. The total plant biomass was higher in control seedlings (~1.7 grams) and lowest in –Fe–P condition (~0.6 grams) (Figure 1F). While, wheat roots under –Fe showed very low allocation of root and the allocation pattern of biomass in –P and –Fe–P plants were similar (Figure 1F). Collectively our data suggests that Fe and P crosstalk and thereby are able to regulate the root characteristic.

The availability of P or Fe was shown to influence the uptake of Fe or P respectively, and perhaps better characterized in *Arabidopsis* (Ward *et al.*, 2008*a*). Nevertheless, this key step for P and Fe in wheat is not well studied. To test the effect of P or Fe availability on P or Fe uptake ICP-MS analysis, Pi uptake, Perl's staining (for Fe) of the roots were performed. As expected, the accumulation of Pi was reduced either in –P or –Fe–P treatments. In our 20 dpt roots, Fe-deficiency does not influence Pi uptake under single –Fe+P deficiency (Figure 2A). In contrast, ICP-MS analysis revealed that only during P-deficiency conditions

significant increase in the accumulation of Fe in the roots was observed compared other treatments (Figure 2B). In addition to this, wheat roots showed higher Zn accumulation under –Fe–P and Mn in +Fe–P condition (Figure 2B). In shoots, only Mn was accumulated in higher amount during –Fe–P. Perl's staining analysis showed no visual presence of Fe in roots under –Fe and –Fe–P conditions (Figure 2C). Enhanced Fe-plaque colorization under –P conditions and mild staining in +Fe+P roots was observed (Figure 2C). This suggests that Fe is aggressively taken up by the plant roots under –P conditions. A key aspect of Fe uptake in cereals is the release of PS for Fe remobilization (Römheld and Marschner, 1986; Römheld, 1991). Accordingly, our assays revealed a high release (42-47 nM) of PS under –Fe condition (10 dpt) (Figure 2D). While, the PS release decreased during –Fe–P condition (16-18 nM) compared to –Fe conditions, significantly higher compared to –P (8-9 nM) and controls (2-3 nM) conditions (Figure 2D). This data indicates that the presence of P is necessary for the wheat roots to respond to Fe deprivation so as to enhance the release of PS.

Comparative analysis of normalized RNAseq expression

Nutrient deficiency alters plant transcriptomes. We recently showed that Fe deprivation results in important global gene expression reprogramming in wheat (Kaur *et al.*, 2019). But how combined Fe and P influence transcriptome remains unknown. Therefore, we set out to gain insight of the transcriptional responseupon combined Fe and P deficiency stress (20 dpt) through RNAseq. In all, 240,013,343 million quality filtered reads with 89% reads having quality score >= Q30 were used for the differential expression analysis using the Kallisto-DESeq2 pipeline (Bray et al., 2016; Love et al., 2014). In response to –P condition, 2983 and 802 genes were downregulated and upregulated respectively (Figure 3A, Table S2). Fe–P combined stress cause an upregulation and downregulation of 1829 genes and 951 genes respectively (Table S2). Refined analysis of our previous –Fe transcriptome subsequently identified 2055 up- and 2191 downregulated genes as –Fe response w.r.t. control (Figure 3A) (Kaur *et al.*, 2019), the Venn diagram revealed those genes that are unique or commonly regulated by Fe and P (Figure 3B and Table S3, S4). Finally, clustered heatmap analysis of all 4 transcriptomes revealed that the transcriptome of control and –Fe–P plants were closer, and distant from those of single Fe or P deficiency conditions (Figure S1A & B). Furthermore, clustered heatmap analysis of the top upregulated genes (top 100 genes) across all treatments suggested that expression of these genes was similar in –Fe and –Fe–P conditions (Figure 3C). In contrast, most of the strongly downregulated genes (left panel)

showed similar patterns during –Fe and –P. This suggest that wheat roots respond to dual deficiency of Fe and P.

Specific and overlapping genes regulated by Fe and/or P deficiency in wheat roots

Under the P-deficiency, wheat induces genes for key transcription factors (Table S5) including PHOSPHATE STARVATION RESPONSE (PHR) homologs and its targets such as PHO1;H1, TaIPS1. Phosphatase related genes like phosphate starvation-induced gene 2 (PS2) were induced, whereas downregulation of PURPLE ACID PHOSPHATASE (PAP) and UDP-GLYCOSYLTRANSFERASES genes was noted (Table S2). Additionally, SPX domain genes also showed induced expression. Our analysis confirmed the P-deficiency response in wheat roots. In contrast, 8 genes encoding for UDP-GLYCOSYLTRANSFERASE were induced during –Fe–P. Glutathione S-transferase, NBS-LRR family, chaperone related genes, ABC and ion transporters were also highly expressed in response to –Fe–P. Additionally, three putative nitrate transporters-NRT (TraesCS5A02G388000; TraesCS7A02G428500; TraesCS3B02G285900) and a gene encoding for nitrate reductase were remarkably downregulated. These expression responses marked the characteristic–Fe–P response in wheat roots along with the downregulation of stress responsive genes including hydrolase and ATP binding proteins (Table S2). Phytohormone genes such as auxin pathway and including PIN and IAA sub-family genes were significantly expressed in –Fe–P (Figure 4A, Table S6). Overall, our data indicates that auxin biosynthesis and secondary metabolism genes for lignification were highly active in the –Fe–P that could support the root phenotype (Figure S2). Interestingly, the overlapping response of transcripts altered during –P and –Fe–P was found to be very low (15.79%), and included multiple PSR responsive/regulated genes (Figure 4B, Table S7). Total of 39 genes were commonly upregulated specifically by –P and –Fe–P. Genes encoding for Glycine-rich cell wall structural proteins were highly upregulated in both conditions (Table S8). In contrast, 110 genes were commonly downregulated during these two conditions. Among the common list peroxidase and proteases were highly repressed. 206 genes showed contrasting expression in –P and –Fe–P, with number of germin-like protein encoding transcripts, and GDSL esterase, CytP450, Glutathione S-Transferase and ABC transporters (Table S8).

Interestingly, the overlapping response of transcripts specifically during –Fe and –Fe–P was found to be comparatively high (24.96%). Comparative –Fe (Kaur *et al.*, 2019) and –Fe–P transcriptome analysis revealed that 83.65% of–Fe alone DEGs were no longer

differentially expressed under the combined –Fe–P treatment (Figure 4C). This suggests that plant use reprogrammed pathways to respond in dual nutrient deficiency as compared to response during single deficiency stress. In total, 494 genes were coregulated irrespective of presence or absence of P, among these 84 genes were observed to be significantly altered in all three deficiency conditions. While 410 genes were commonly regulated by Fe-deficiency, either upregulated (i.e. nicotianamine synthase genes-NAS, basic helix loop helix-bHLH and WRKY transcription factors, and transporters viz., ZIFL, YSL, NRT1) or repressed (i.e. ABC-G family peroxidases, arabinogalactan protein encoding, sulfate transporter, ferritin and loricrin like genes) regardless of P status in the growth medium. 200 genes showed opposite expression pattern mainly including no apical-meristem (NAC) domain containing, cobalt-ion protein encoding , glycosyltransferases and zinc transporter genes were marked by this category (Table S9).

During –Fe or in –Fe–P, multiple genes involved in Fe homeostasis were induced suggesting that presence of P does influence the expression of Fe related genes. Furthermore, 93 Fe starvation responsive genes (FSR; Strategy I and II) were checked for their expression response (Table S7). Most of the FSR genes showed downregulation in P-deficiency, but were upregulated either in –Fe+P or –Fe–P (Figure 4D). Up-regulated genes also included those involved in biosynthesis of PS *via* methionine cycle. Lastly, 84 genes were commonly altered in all three growth conditions i.e. +Fe–P, –F+P and –Fe–P (Table S9). Only one fourth of these genes were significantly commonly upregulated such as WRKY transcription factor and genes encoding SPX domain containing protein. 62 genes were downregulated including ABC-G family, and TaYSL12 encoding genes.

KEGG pathway enrichment analysis of DEGs and metabolome analysis

Mapman based analysis suggest that high expression of genes involved in UDP-glycosyl-transferases and GST related pathways during –Fe–P, when compared to other treatments and controls (Figure 5A). Overall, our data indicates that auxin biosynthesis and secondary metabolism genes for lignification were highly active in –Fe–P response (Figure S2, S4). To further categorise the DEGs from each nutritional growth conditions in their corresponding metabolic pathways we mapped them to the KEGG database. Our analysis revealed that in response to P-deficiency (+Fe–P), genes related to phenylpropanoid pathway, photosynthesis, ABC transporters, and genes for nitrogen metabolism were highly enriched (Figure 5B). In response to –Fe–P conditions, enrichment of genes involved in glutathione metabolism,

glycerophospholipid metabolism, starch and sucrose metabolism and galactose metabolism pathways and cysteine and methionine metabolism was observed (Figure 5B). Interestingly, enrichment of cysteine and methionine metabolism genes was also observed in response to –Fe+P treatment (Kaur *et al.*, 2019), indicating that the enrichment of genes is Fe specific, and independent of P status.

To further study the role of primary metabolites during the Fe and P interaction GC-MS analysis was done using the fresh roots of the wheat seedlings post 20 dpt. Our analysis showed that significant variation in the accumulation of metabolites between nutrient-deficient and nutrient-sufficient plants along with a variation amongst nutrient deficiency treatments (Figure 6A, Table S10). While suppression of oxalic acid and increase in 4-ketoglucose levels was unique for –P treatment, the increase in fumaric acid and myo-inositol marked metabolic change was specific for –Fe conditions. A contrasting level of serine and succinic acid in +Fe–P (low) and –Fe+P (high) was found to be normalized in dual deficiency with respect to control. The –Fe–P conditions is characterized by specific metabolic changes marked by decrease in acetic acid, butanoic acid, valine, threonine and glucofuranoside levels and increased accumulation of β-amino-isobutyric acid, strearic acid, arabinonic acid and aconitic acid. Nevertheless, numerous metabolitesdecreased commonly in –Fe–P and –Fe conditions such as aspartic acid, hexonic acid, glucose cystathione and, alanine. While the acids showed high accumulation in –Fe they were highly reduced during –Fe–P. The metabolites that decrease in –Fe–P appeared to follow the same trends in –P conditions including citric acid and hexapyranose. Finally, sugars,sugar conjugates (i.e. d-ribofuranose, a-d-galactopyranoside, a-d-mannopyranoside), amino acids (i.e. b-aminoisobutyric acid, cystathione and L-alanine),aconitic acid and arabinonic were predominant in –Fe–P conditions (Figure 6B).

Enrichment of Fe responsive cis-regulatory elements in regulated genes

To get an insight into the regulatory function of the expressed genes during single (–Fe, –P) and combined (–Fe–P) nutrient stress, Fe responsive cis-regulatory elements were analysed. Our analysis revealed multiple TFs that are predominantly expressed in -Fe-P condition as compared to P-deficiency (Table S5, Figure S5). Especially, genes encoding for multiple bHLH, C2H2 and NAC TFs were highly represented in –Fe–P. Earlier the comprehensive resource of new putative frequent cis-regulatory elements (freq-pCREs) were identified in the gene clusters responsive for Fe-deficiency in roots (Ivanov *et al.*, 2012; Schwarz *et al.*, 2020).

Herein we included genes differentially regulated in response to the deficiency of Fe and/or P. To optimize and validate our analysis, we used three control sets of genes (~100) with log2FC between -0.5 and 0.5 in –Fe w.r.t to control and checked for the occurrence of freq-pCREs in their promoters. All the random sets behaved in a similar pattern with low presence of these elements (Table S11). Our analysis identified that differentially accumulated transcripts are enriched with the uniform percentage distribution of freq-pCREs. To address the mechanistic understanding of Fe responsive freq-CREs, analysis wasdone in subset of FSR genes and PSR genes. Interestingly, when FSR and PSR related genes were analysed this balance was found to be perturbed. The dominance and biasness of freq-pCREs was observed significantly in Fe deficiency (Table 1). For example, cis-domains such as AAGTA, ACTAGT, CACACG, AATTGC and CGTGCC were present in higher proportion in Fe-deficiency responsive genes as compared to P deficiency. Our work revealed an overlapping response of DEGs during Fe and P deficiency as freq-pCREs were highly enriched in Fe-deficiency and was present in the promoters of P response related genes. Similarly, cis-element for phosphate responsive region such as P1BS (PHR1 binding sequences, GNATATNC) was present at 62% of the PSR and 23.66% of FSR genes (Table S12). Interestingly, P1BS motif was present 34.97, 34,61% and 36.91% in the promoter regions of DGEs in response to –Fe+P, +Fe–P and –Fe–P respectively.

Effect of prolonged Fe and P deficiency on the panicle development

So far, investigation of Fe and P focused on their individual and combined effect in model plants. But, how long-term Fe and/or P deficiencies affects late stage of crop is largely unknown. Therefore, we assessed the physiological and molecular responses of wheat plants subjected to prolonged periods and effect of Fe and P deficiency (Figure 7A). In 55 days old wheat plants, Fe-deficiency causes the most severe effects on productivity, spike length, and rachis development compared to other treatments (Figure 7B & C). Strikingly, Fe starved plants showed significant decrease in the length of awn and rachis. The above-mentioned developmental effects were less predominant under prolonged –P condition. Interestingly, the negative effect of prolonged exposure of Fe deprivation on spikelet development is rescued by the –Fe–P treatment. Our result show that removal of P along with Fe was able to rescue the growth retardation in spike and related characteristic. Overall, our data suggest that the inhibitory effect caused by Fe-deficiency on wheat development could be minimized by subjecting the seedlings to P deprivation.

DISCUSSION

Fe and P are essential elements for plants, utilized in nearly every cellular process. In crops, there is limited understanding of the interaction between Fe and P homeostasis to coordinate physiological and molecular response. The current work aimed to fill this knowledge gap by providing first insight on wheat response to Fe and/or P deficiency stresses. Our data showed that P-deficiency compensates Fe negative effect on wheat growth and development such as root growth and spike development. Our transcriptome analysis suggests the enriched presence of putative Fe responsive cis-regulatory binding sites. By combining transcriptome and metabolome analysis, we revealed a specific component underlying during Fe and P combined stress response in wheat.

To sustain the Fe or P deficiency in soil, crop plants like rice, maize and soybeans have adapted multiple strategy responses so as to maximize their survival under depleted soils. But how crop plant responds to co-occurring Fe and P stress remains poorly understood. Our study revealed that Fe uptake is dependent on P status in the rhizospheric region. The enhanced accumulation of Fe could be accounted for by the continued expression of Strategy-II related genes (Figure 2D and Figure S3B). These observations are in line with early work where we showed that wheat use Strategy-II genes to respond to Fe-deficiency (Kaur *et al.*, 2019). Genes expressed in response to –Fe and –Fe–P reinforce thus that wheat primarily uses Strategy-II mode for Fe uptake even during changing regimes of P. For instance, the relatively high release of PS and gene expression patterns of certain specific YSL, metal transporters and a few TFs involved in metal homeostasis either in –Fe or –Fe–P confirms that wheat primarily utilizes Strategy-II mode of Fe uptake route to mobilize Fe from roots to shoots even under P-deficiency (Figure S3) (Kumar *et al.*, 2019; Kaur *et al.*, 2019). Under P-deficiency, wheat decreases citrate levels, and increases expression of citrate synthase that could subsequently favor citrate exudation and this could be one important mechanism for higher Fe accumulation under P-deficiency (Table S10 and Figure 6A). On the other hand, Fe-deficient wheat roots tend to accumulate high levels of citrate with downregulation of citrate synthase transcript (TraesCS7A02G409800). Citrate being an Fe(III) chelator has been reported to play a relevant role in iron acquisition and xylem Fe transport (Durrett *et al.*, 2007; Valentinuzzi *et al.*, 2015). Our transcriptome changes support these metabolic changes. Indeed, P-deficiency showed an increase in transcript abundance of citrate synthase (TraesCS4A02G142400) that further supports the speculation of citrate exudation. Overexpression of citrate synthase has been shown to support plant growth under

P-deficiency by increasing citrate exudation (Anoop *et al.*, 2003). Furthermore, our OMICs study revealed that oxalate, fumarate and aconitate that accumulated specifically under P, Fe and dual deficiency respectively suggest distinct TCA cycle programming and energy balance (Igamberdiev and Kleczkowski, 2019). Our data further confirmed that plants accumulate/release of organic acids, mainly malate and citrate under P and Fe deficiencies to the rhizospheric regions for efficient mineralization (Kania et al., 2003; Ligaba et al., 2004; Wu, Liu, Riaz, Yan, & Jiang, 2019; Zhang et al., 2015; Kania, Langlade, Martinoia, & Neumann, 2003; Mimmo et al., 2014).). The cross-talk between P and Fe to regulate Fe uptake and transport has been also reported in dicots, such as *Arabidopsis*. For instance, P-deficiency was shown to induce expression of Fe homeostasis related genes like AtFRO2, AtIRT1 and ferritin genes (*Atfer1*) (Misson et al., 2005; Y.-H. Wang, Garvin, & Kochian, 2002;Bournier et al., 2013). Likewise, Fe-deficiency can induce expression of P acquisition genes (Thimm *et al.*, 2004; Lucena *et al.*, 2019). These evidences along with our observations reinforce a strong link between the molecular interactions between P and Fe homeostasis in crops.

Identifying the specific signatures for the dual deficiency of –Fe and –P will provide an important link for homeostatic interaction between micro and macronutrient interaction. This study led to the identification of specific signatures at the transcript and metabolome level. In plants phenylpropanoid pathway (PPP) is the source of numerous phenylalanine derivatives involved in multiple development and physiological process, including lignin biosynthesis and cell wall development (Douglas, 1996; Boerjan *et al.*, 2003). The role of glycosyltransferases has been demonstrated to efficiently control the phenylpropanoid pathway (Aksamit-Stachurska *et al.*, 2008). The high expression of UGT transcripts during –Fe–P suggest reorganization of metabolic pathways that resulted in the identification of molecular signatures. Our MapMan analysis reinforces this, wherein high expression was observed for genes, especially encoding for simple phenols, lignin biosynthesis, isoflavonoids and carotenoids (Figure S2B). Multiple transcripts encoding for peroxidases, dirigent proteins and one laccase were also highly up-regulated in –Fe–P treatment (Table S2). This led to the speculation that dirigent-guided lignin deposition might be up-regulated in the roots during this combinatorial deficiency of Fe and P. Dirigent proteins in plants are well known to modulate cell wall metabolism during abiotic and biotic stress exposure (Paniagua *et al.*, 2017). The high cell wall related activity in wheat roots could be correlated with the enhanced root biomass allocation (Figure 1F). Previously it was observed that lignin

biosynthesis could be linked with the excess Fe related responses to provide tolerance in rice (Stein *et al.*, 2019). The confirmatory role of lignification needs the functional attention in wheat to address this under dual deficiency. In addition to that Cytochrome P450, a key player in plant development, biotic and abiotic stresses (Narusaka *et al.*, 2004). These gene families are also considered as a scaffold-proteins for the lignin biosynthesis. Based on our analysis, including physiological and biochemical, increased lignification process in the roots during the –Fe–P condition could be one of the important biochemical hallmarks.

KEGG enrichment analysis reinforced our finding that genes encoding for glutathione metabolism were significantly enriched during –Fe–P treatment. Glutathione levels, its metabolism and activity have been correlated with the tolerance for –Fe (Zaharieva and Abadia, 2003; Bashir *et al.*, 2007; Kaur *et al.*, 2019). The increased burst of glutathione metabolism related genes provide evidence that graminaceous and Eucoids plants under –Fe–P show a very high glutathione related metabolism to compensate for the Fe-deficiency. Other components such as nitric oxide-mediated iron uptake response is also controlled by the supply of glutathione (Shanmugam *et al.*, 2015). The robust expression of glutathione related genes in –Fe–P condition suggest that the plants are undergoing through a strong redox process that is required to survive under combinatorial deficiency. Accumulation of glycine and serine has been implicated to negatively affect root length and nitrate uptake in *Brassica campestris* .Our data from this and previous study for contrasting levels of glycine and serine accumulation could explain the short roots during –Fe compared to +Fe+P, –P and –Fe –P (Kaur *et al.*, 2019). Glycine can induce ethylene guided inhibition of root elongation or it could be converted into amino butyric acid moieties during stress (Han *et al.*, 2018; Igamberdiev and Kleczkowski, 2019).

In contrast to during Fe-deficiency, we have observed an increase in the root growth and biomass under P-deficiency, which was maintained in response dual deficiency i.e. –Fe–P. Worth to mention that in the model plant, the opposite situation was observed. Short primary root under –P and recovery by –P–Fe (Bouain et al., 2019). This indicate that dicots and monocots have evolved distinct genetic programs to respond to single and/or combined nutrient stress. While most of the studies pertaining to the nutrient interaction have been limited to the vegetative stage, there are limited studies on the molecular basis regulating co-occurring nutrients deficiency during the reproductive stage. Individual nutrient Fe or P stress in crops including wheat affects the overall physiological growth and development; and yield

components (Clark *et al.*, 1988; Carstensen *et al.*, 2018). Our study further confirmed that deficiency of either P or Fe largely impacts plant productivity, with Fe-deficiency causing more impact when compared to P. More importantly, we showed that Fe-deficiency induced morphological changes (i.e. spikelets and roots) that can be restored by removing P from the growth solution. For instance, we revealed that the drastic effect of single -Fe was rescued by the dual starvation (-Fe-P). This remained true for the morphology for spikelet, rachis and awn (Figure 7C). The drastic reduction in the length of awn, rachis in turn could the grain yields. In tobacco, it has been proven that inhibiting Fe uptake and transport can induce morphological abnormalities including infertility (Takahashi *et al.*, 2003). The inhibitory effect of –Fe was rescued by the dual deficiency of Fe and P, suggesting the removal of macronutrient such as P could minimize the impact of Fe-deficiency. Also, it is clear that understanding how plants integrate P and Fe signals to controls plant development at reproductive stage is at it is early stage. Our data opens new research avenues to uncover the molecular basis of P and Fe signalling crosstalk in plants, and will lead to designing strategies to develop wheat cultivars with an improved Fe and P use efficiency.

ACKNOWLEDGEMENTS

The authors thank Executive Director, NABI for facilities and support. This work was funded by the NABI-CORE grant to AKP. GK and VS acknowledge NABI-SRF Fellowships. Technical help from Jagdeep Singh for the GC-MS analysis is highly appreciated. DBT-eLibrary Consortium (DeLCON) is acknowledged for providing timely support and access to e-resources for this work. The wheat genome resources developed by International Wheat Genome Sequencing Consortium are highly appreciated.

REFERENCES

Abadia J, Vazquez S, Rellan-Alvarez R, El-Jendoubi H, Abadia A, Alvarez-Fernandez A, Lopez-Millan AF. 2011. Towards a knowledge-based correction of iron chlorosis. Plant physiology and biochemistry□: PPB **49**, 471–482.

Aggarwal S, Kumar A, Bhati KK, Kaur G, Shukla V, Tiwari S, Pandey AK. 2018. RNAi-Mediated Downregulation of Inositol Pentakisphosphate Kinase (IPK1) in Wheat Grains Decreases Phytic Acid Levels and Increases Fe and Zn Accumulation. Frontiers in plant science **9**, 259.

Aksamit-Stachurska A, Korobczak-Sosna A, Kulma A, Szopa J. 2008. Glycosyltransferase efficiently controls phenylpropanoid pathway. BMC Biotechnology **8**,

25.

Anoop VM, Basu U, McCammon MT, McAlister-Henn L, Taylor GJ. 2003. Modulation of citrate metabolism alters aluminum tolerance in yeast and transgenic canola overexpressing a mitochondrial citrate synthase. Plant physiology **132**, 2205–2217.

Bashir K, Nagasaka S, Itai RN, Kobayashi T, Takahashi M, Nakanishi H, Mori S, Nishizawa NK. 2007. Expression and enzyme activity of glutathione reductase is upregulated by Fe-deficiency in graminaceous plants. Plant molecular biology **65**, 277–284.

Bhati KK, Alok A, Kumar A, Kaur J, Tiwari S, Pandey AK. 2016. Silencing of ABCC13 transporter in wheat reveals its involvement in grain development, phytic acid accumulation and lateral root formation. Journal of experimental botany **67**, 4379–4389.

Boerjan W, Ralph J, Baucher M. 2003. Lignin biosynthesis. Annual review of plant biology **54**, 519–546.

Bouain N, Doumas P, Rouached H. 2016. Recent Advances in Understanding the Molecular Mechanisms Regulating the Root System Response to Phosphate Deficiency in Arabidopsis. Current genomics **17**, 304–308.

Bouain N, Shahzad Z, Rouached A, Khan GA, Berthomieu P, Abdelly C, Poirier Y, Rouached H. 2014. Phosphate and zinc transport and signalling in plants: toward a better understanding of their homeostasis interaction. Journal of Experimental Botany **65**, 5725–5741.

Cai H, Xie W, Zhu T, Lian X. 2012. Transcriptome response to phosphorus starvation in rice. Acta Physiologiae Plantarum **34**, 327–341.

Carstensen A, Herdean A, Schmidt SB, Sharma A, Spetea C, Pribil M, Husted S. 2018. The Impacts of Phosphorus Deficiency on the Photosynthetic Electron Transport Chain. Plant Physiology **177**, 271 LP – 284.

Chutia R, Abel S, Ziegler J. 2019. Iron and Phosphate Deficiency Regulators Concertedly Control Coumarin Profiles in Arabidopsis thaliana Roots During Iron, Phosphate, and Combined Deficiencies . Frontiers in Plant Science **10**, 113.

Clark RB, Williams EP, Ross WM, Herron GM, Witt MD. 1988. Effect of iron deficiency chlorosis on growth and yield component traits of sorghum. Journal of Plant Nutrition **11**, 747–754.

Curie C, Panaviene Z, Loulergue C, Dellaporta SL, Briat J-F, Walker EL. 2001. Maize yellow stripe1 encodes a membrane protein directly involved in Fe(III) uptake. Nature **409**, 346–349.

Dalton CC, Iqbal K, Turner DA. 1983. Iron phosphate precipitation in Murashige and

Skoog media. Physiologia Plantarum **57**, 472–476.

Douglas CJ. 1996. Phenylpropanoid metabolism and lignin biosynthesis: from weeds to trees. Trends in Plant Science **1**, 171–178.

Durrett TP, Gassmann W, Rogers EE. 2007. The FRD3-Mediated Efflux of Citrate into the Root Vasculature Is Necessary for Efficient Iron Translocation. Plant Physiology **144**, 197 LP – 205.

Han R, Khalid M, Juan J, Huang D. 2018. Exogenous glycine inhibits root elongation and reduces nitrate-N uptake in pak choi (Brassica campestris ssp. Chinensis L.). PLOS ONE **13**, e0204488.

Heuer S, Gaxiola R, Schilling R, Herrera-Estrella L, López-Arredondo D, Wissuwa M, Delhaize E, Rouached H. 2017. Improving phosphorus use efficiency: a complex trait with emerging opportunities. The Plant Journal **90**, 868–885.

Hirsch J, Marin E, Floriani M, Chiarenza S, Richaud P, Nussaume L, Thibaud MC. 2006. Phosphate deficiency promotes modification of iron distribution in Arabidopsis plants. Biochimie **88**, 1767–1771.

Igamberdiev AU, Kleczkowski LA. 2019. Thermodynamic buffering, stable non-equilibrium and establishment of the computable structure of plant metabolism. Progress in Biophysics and Molecular Biology **146**, 23–36.

Inoue H, Kobayashi T, Nozoye T, Takahashi M, Kakei Y, Suzuki K, Nakazono M, Nakanishi H, Mori S, Nishizawa NK. 2009. Rice OsYSL15 is an iron-regulated iron(III)-deoxymugineic acid transporter expressed in the roots and is essential for iron uptake in early growth of the seedlings. The Journal of biological chemistry **284**, 3470–3479.

Ivanov R, Brumbarova T, Bauer P. 2012. Fitting into the Harsh Reality: Regulation of Iron-deficiency Responses in Dicotyledonous Plants. Molecular Plant **5**, 27–42.

Kania A, Langlade N, Martinoia E, Neumann G. 2003. Phosphorus deficiency-induced modifications in citrate catabolism and in cytosolic pH as related to citrate exudation in cluster roots. Plant and Soil **248**, 117–127.

Kaur G, Shukla V, Kumar A, *et al.* 2019. Integrative analysis of hexaploid wheat roots identifies signature components during iron starvation. Journal of experimental botany **70**, 6141–6161.

Kobayashi T, Nishizawa NK. 2012. Iron uptake, translocation, and regulation in higher plants. Annual review of plant biology **63**, 131–152.

Kumar A, Kaur G, Goel P, Bhati KK, Kaur M, Shukla V, Pandey AK. 2019. Genome-wide analysis of oligopeptide transporters and detailed characterization of yellow stripe

transporter genes in hexaploid wheat. Functional & integrative genomics **19**, 75–90.

Lee S, Chiecko JC, Kim SA, Walker EL, Lee Y, Guerinot M Lou, An G. 2009. Disruption of OsYSL15 Leads to Iron Inefficiency in Rice Plants. Plant Physiology **150**, 786 LP – 800.

Ligaba A, Shen H, Shibata K, Yamamoto Y, Tanakamaru S, Matsumoto H. 2004. The role of phosphorus in aluminium-induced citrate and malate exudation from rape (Brassica napus). Physiologia plantarum **120**, 575–584.

Livak KJ, Schmittgen TD. 2001. Analysis of relative gene expression data using real-time quantitative PCR and the 2(-Delta Delta C(T)) Method. Methods (San Diego, Calif.) **25**, 402–408.

Love MI, Huber W, Anders S. 2014. Moderated estimation of fold change and dispersion for RNA-seq data with DESeq2. Genome Biology **15**, 550.

Lucena C, Porras R, García MJ, Alcántara E, Pérez-Vicente R, Zamarreño ÁM, Bacaicoa E, García-Mina JM, Smith AP, Romera FJ. 2019. Ethylene and Phloem Signals Are Involved in the Regulation of Responses to Fe and P Deficiencies in Roots of Strategy I Plants . Frontiers in Plant Science **10**, 1237.

Ma JF, Ling H-Q. 2009. Iron for plants and humans. Plant and Soil **325**, 1–3.

Marschner H. 1995. 9 - Functions of Mineral Nutrients: Micronutrients. In: Marschner HBT-MN of HP (Second E, ed. London: Academic Press, 313–404.

Mimmo T, Del Buono D, Terzano R, Tomasi N, Vigani G, Crecchio C, Pinton R, Zocchi G, Cesco S. 2014. Rhizospheric organic compounds in the soil–microorganism–plant system: their role in iron availability. European Journal of Soil Science **65**, 629–642.

Misson J, Raghothama KG, Jain A, *et al.* 2005. A genome-wide transcriptional analysis using Arabidopsis thaliana Affymetrix gene chips determined plant responses to phosphate deprivation. Proceedings of the National Academy of Sciences of the United States of America **102**, 11934–11939.

Mollier A, Pellerin S. 1999. Maize root system growth and development as influenced by phosphorus deficiency. Journal of Experimental Botany **50**, 487–497.

Mora-Macías J, Ojeda-Rivera JO, Gutiérrez-Alanís D, Yong-Villalobos L, Oropeza-Aburto A, Raya-González J, Jiménez-Domínguez G, Chávez-Calvillo G, Rellán-Álvarez R, Herrera-Estrella L. 2017. Malate-dependent Fe accumulation is a critical checkpoint in the root developmental response to low phosphate. Proceedings of the National Academy of Sciences **114**, E3563 LP-E3572.

Morrissey J, Guerinot M Lou. 2009. Iron uptake and transport in plants: the good, the bad,

and the ionome. Chemical reviews **109**, 4553–4567.

Murata Y, Ma JF, Yamaji N, Ueno D, Nomoto K, Iwashita T. 2006. A specific transporter for iron(III)–phytosiderophore in barley roots. The Plant Journal **46**, 563–572.

Narayanan, A. Reddy K. 1982. Effect of phosphorus deficiency on the form of plant root system. Slough, UK□: Commonwealth Agricultural Bureaux, c1982., 412–417.

Narusaka Y, Narusaka M, Seki M, Umezawa T, Ishida J, Nakajima M, Enju A, Shinozaki K. 2004. Crosstalk in the responses to abiotic and biotic stresses in Arabidopsis: analysis of gene expression in cytochrome P450 gene superfamily by cDNA microarray. Plant molecular biology **55**, 327–342.

Naumann C, Müller J, Sakhonwasee S, Wieghaus A, Hause G, Heisters M, Bürstenbinder K, Abel S. 2019. The Local Phosphate Deficiency Response Activates Endoplasmic Reticulum Stress-Dependent Autophagy. Plant Physiology **179**, 460 LP – 476.

Nozoye T, Nagasaka S, Kobayashi T, Takahashi M, Sato Y, Sato Y, Uozumi N, Nakanishi H, Nishizawa NK. 2011. Phytosiderophore efflux transporters are crucial for iron acquisition in graminaceous plants. Journal of Biological Chemistry **286**, 5446–5454.

Oono Y, Kobayashi F, Kawahara Y, Yazawa T, Handa H, Itoh T, Matsumoto T. 2013. Characterisation of the wheat (Triticum aestivum L.) transcriptome by de novo assembly for the discovery of phosphate starvation-responsive genes: gene expression in Pi-stressed wheat. BMC genomics **14**, 77.

Paniagua C, Bilkova A, Jackson P, *et al.* 2017. Dirigent proteins in plants: modulating cell wall metabolism during abiotic and biotic stress exposure. Journal of experimental botany **68**, 3287–3301.

Quanbeck S, Brachova L, Campbell A, *et al.* 2012. Metabolomics as a Hypothesis-Generating Functional Genomics Tool for the Annotation of Arabidopsis thaliana Genes of "Unknown Function" . Frontiers in Plant Science **3**, 15.

Raghothama KG. 1999. PHOSPHATE ACQUISITION. Annual Review of Plant Physiology and Plant Molecular Biology **50**, 665–693.

Ritchie ME, Phipson B, Wu D, Hu Y, Law CW, Shi W, Smyth GK. 2015. limma powers differential expression analyses for RNA-sequencing and microarray studies. Nucleic acids research **43**, e47–e47.

Römheld V. 1991. The role of phytosiderophores in acquisition of iron and other micronutrients in graminaceous species: An ecological approach. Plant and Soil **130**, 127–134.

Römheld V, Marschner H. 1986. Evidence for a specific uptake system for iron

phytosiderophores in roots of grasses. Plant physiology **80**, 175–180.

Rouached H, Arpat AB, Poirier Y. 2010. Regulation of phosphate starvation responses in plants: signaling players and cross-talks. Molecular plant **3**, 288–299.

Schwarz B, Azodi CB, Shiu S-H, Bauer P. 2020. Putative cis-Regulatory Elements Predict Iron Deficiency Responses in Arabidopsis Roots. Plant Physiology **182**, 1420 LP – 1439.

Secco D, Bouain N, Rouached A, Prom-U-Thai C, Hanin M, Pandey AK, Rouached H. 2017. Phosphate, phytate and phytases in plants: from fundamental knowledge gained in Arabidopsis to potential biotechnological applications in wheat. Critical reviews in biotechnology **37**, 898–910.

Secco D, Jabnoune M, Walker H, Shou H, Wu P, Poirier Y, Whelan J. 2013. Spatio-temporal transcript profiling of rice roots and shoots in response to phosphate starvation and recovery. The Plant cell **25**, 4285–4304.

Shanmugam V, Wang Y-W, Tsednee M, Karunakaran K, Yeh K-C. 2015. Glutathione plays an essential role in nitric oxide-mediated iron-deficiency signaling and iron-deficiency tolerance in Arabidopsis. The Plant Journal **84**, 464–477.

Shimizu A, Yanagihara S, Kawasaki S, Ikehashi H. 2004. Phosphorus deficiency-induced root elongation and its QTL in rice (Oryza sativa L.). Theoretical and Applied Genetics **109**, 1361–1368.

Soneson C, Love MI, Robinson MD. 2015. Differential analyses for RNA-seq: transcript-level estimates improve gene-level inferences. F1000Research **4**, 1521.

Stein RJ, Duarte GL, Scheunemann L, Spohr MG, de Araújo Júnior AT, Ricachenevsky FK, Rosa LMG, Zanchin NIT, Santos RP dos, Fett JP. 2019. Genotype variation in rice (Oryza sativa l.) tolerance to fe toxicity might be linked to root cell wall lignification. Frontiers in Plant Science **10**, 1–20.

Svistoonoff S, Creff A, Reymond M, Sigoillot-Claude C, Ricaud L, Blanchet A, Nussaume L, Desnos T. 2007. Root tip contact with low-phosphate media reprograms plant root architecture. Nature Genetics **39**, 792–796.

Takagi S. 1976. Naturally occurring iron-chelating compounds in oat- and rice-root washings. Soil Science and Plant Nutrition **22**, 423–433.

Takahashi M, Terada Y, Nakai I, Nakanishi H, Yoshimura E, Mori S, Nishizawa NK. 2003. Role of nicotianamine in the intracellular delivery of metals and plant reproductive development. The Plant cell **15**, 1263–1280.

Thimm O, Bläsing O, Gibon Y, Nagel A, Meyer S, Krüger P, Selbig J, Müller LA, Rhee SY, Stitt M. 2004. mapman: a user-driven tool to display genomics data sets onto diagrams

of metabolic pathways and other biological processes. The Plant Journal **37**, 914–939.

Valentinuzzi F, Pii Y, Vigani G, Lehmann M, Cesco S, Mimmo T. 2015. Phosphorus and iron deficiencies induce a metabolic reprogramming and affect the exudation traits of the woody plant Fragaria×ananassa. Journal of Experimental Botany **66**, 6483–6495.

Wang Y-H, Garvin DF, Kochian L V. 2002. Rapid induction of regulatory and transporter genes in response to phosphorus, potassium, and iron deficiencies in tomato roots. Evidence for cross talk and root/rhizosphere-mediated signals. Plant physiology **130**, 1361–1370.

Ward JT, Lahner B, Yakubova E, Salt DE, Raghothama KG. 2008*a*. The effect of iron on the primary root elongation of Arabidopsis during phosphate deficiency. Plant Physiology **147**, 1181–1191.

Ward JT, Lahner B, Yakubova E, Salt DE, Raghothama KG. 2008*b*. The effect of iron on the primary root elongation of Arabidopsis during phosphate deficiency. Plant physiology **147**, 1181–1191.

Wickham H. 2017. Book review: ggplot2 – Elegant Graphics for Data Analysis (2nd Edition). , 2–5.

Wu X, Liu G, Riaz M, Yan L, Jiang C. 2019. Metabolic changes in roots of trifoliate orange [Poncirus trifoliate (L.) Raf.] as induced by different treatments of boron deficiency and resupply. Plant and Soil **434**, 217–229.

Xie X, Hu W, Fan X, Chen H, Tang M. 2019. Interactions Between Phosphorus, Zinc, and Iron Homeostasis in Nonmycorrhizal and Mycorrhizal Plants. Frontiers in plant science **10**, 1172.

Zaharieva TB, Abadia J. 2003. Iron deficiency enhances the levels of ascorbate, glutathione, and related enzymes in sugar beet roots. Protoplasma **221**, 269–275.

Zhang F, Sun Y, Pei W, *et al.* 2015. Involvement of OsPht1;4 in phosphate acquisition and mobilization facilitates embryo development in rice. The Plant journal□: for cell and molecular biology **82**, 556–569.

Zhou Y, Neuhäuser B, Neumann G, Ludewig U. 2020. LaALMT1 mediates malate release from phosphorus-deficient white lupin root tips and metal root to shoot translocation. Plant, Cell & Environment **n/a**.

Zhu A, Ibrahim JG, Love MI. 2018. Heavy-tailed prior distributions for sequence count data: removing the noise and preserving large differences. Bioinformatics **35**, 2084–2092.

Table 1: Percentage distribution of top twenty putative frequent cis-regulatory elements (freq-pCREs) analyzed in the RNAseq data (–Fe+P, +Fe–P, –Fe–P) and in shortlisted genes involved during Fe-starvation response (FSR-93 genes) and phosphate starvation response (PSR-50 genes). Detailed list of freq-pCREs analysis is shown in Table S11.

pCREs (motifs)	**Percentage distribution of freq-pCREs in given condition**					**Top TF family**
	-Fe+P	**+Fe-P**	**-Fe-P**	**FSR**	**PSR**	
CATGCA	63.82	62.22	65.79	**80.65**	80.00	ABI3VP1
ATGCAT	64.20	64.68	65.72	**76.34**	70.00	B3
GCATGA	46.09	44.41	46.91	**68.82**	60.00	B3
ATATAT	65.87	66.42	67.52	**66.67**	70.00	ARID
AAACTA	49.29	50.49	50.65	**59.14**	66.00	ARID
TATGCA	45.24	46.50	47.05	**58.06**	50.00	ABI3VP1
AATTAA	54.52	55.30	54.21	**54.84**	56.00	Homeobox
AAAGTA	42.53	43.28	41.33	**53.76**	32.00	C2C2-Dof
ACTAGT	43.24	41.80	41.73	**50.54**	32.00	bHLH
AATATG	49.27	49.64	48.02	**49.46**	52.00	G2-like
CACACG	43.24	42.03	42.95	**49.46**	28.00	BZR
TAATTA	48.02	50.36	49.60	**47.31**	54.00	Homeobox
AGCATG	44.21	44.65	45.07	**46.24**	52.00	B3
AGGCAT	33.58	34.35	33.71	**45.16**	38.00	G2-like
AATTGC	37.12	39.23	36.29	**44.09**	26.00	Homeobox
CCGGCC	50.82	49.48	50.40	**44.09**	58.00	GeBP
CGGCCG	48.59	47.03	46.15	**44.09**	54.00	GeBP
AGTCAA	38.93	38.39	40.00	**41.94**	58.00	WRKY
CGTGCC	35.68	33.08	34.78	**41.94**	30.00	bHLH
ACGAAA	37.00	36.46	37.16	**40.86**	28.00	NLP

LEGENDS FOR FIGURES:

Figure 1: Effect of Fe and P on the growth of roots and shoots of wheat seedlings exposed to the mentioned condition for the period of 5, 10 and 20 days. (A) Experimental setup and the overall growth of wheat seedlings in the given conditions. Morphology of the wheat seedlings subjected to mentioned stress condition (+Fe+P, +Fe–P, –Fe+P and –Fe-P). Pictures were taken after 5, 10, 20 days. (B) Representative root phenotype of wheat roots after 20 days of treatment. (C) Primary root length of wheat seedlings under treated conditions. (D) Total number of 1st order lateral roots and (E) Average total length of lateral roots (n=8). (F) Fresh biomass of the root and shoots of the seedlings (S-shoots; R-roots). # and * indicates significant difference at $p<0.05$ and $p<0.01$ respectively.

Figure 2: **Effect of Fe and P interaction on metal accumulation and its mobilization.** (A) Phosphate uptake in the seedlings of wheat under different regimes of Fe and P. (B) Metal concentration in roots and shoots of wheat seedling subjected to –Fe, –Pi and –Fe–Pi stress. (C) Phenotype of wheat root seedlings during the combinatorial effects of Fe and P as observed by the Perl's Stain for iron plaque (blue plaques). (D) Estimation of the phytosiderophore release by the wheat roots under the mentioned condition. # and * indicates significant difference at $p<0.05$ and $p<0.01$ respectively.

Figure 3: Transcriptome analysis of wheat roots grown under single (-P, -Fe) and dual (-Fe-P) conditions. (A) Genes differentially expressed in response to different deficiency conditions (Dual, -Fe-P; P deficiency, +Fe–P; Fe deficiency, –Fe+P) w.r.t. Control wheat roots. (B) Venn diagram representing the number of unique as well as common differentially regulated genes for the three conditions w.r.t. Control. (C) Analysis of highest differentially responsive genes during –Fe–P condition. Increasing intensities of red and blue colors represent up- and downregulation, as depicted by the color scale.

Figure 4: Fe deficiencyresponsive transcripts affected by different regimes of P. (A) Heatmap analysis of 60 genes involved in the auxin biosynthesis and response during –P, –Fe and –Fe –P. (B) Analysis of PSR related genes during Fe deficiency (-Fe) and combinatorial deficiency –Fe–P. In total 50 PSR related DEGs belonging to the category of uptake, transport and regulation were used for the analysis. (C) Effect of additional P deficiency on Fe responsive genes. Inner circle of the sunburst graph represents transcripts up- and downregulated under Fe stress while outer concentric circle represents the distribution of said these genes upon dual combined stress. (UP: upregulated; Down: Downregulated; Dual_no: not DE under –Fe–P). (D) Heatmap analysis of 93 iron responsive DEGs involved in Fe uptake, mobilization and regulation (identified from Kaur et al., 2019) during –P and –Fe –P.

Figure 5: Mapman and KEGG Pathway enrichment analysis. (A) Detailed analysis of DEGs for UDP glycosyltransferases, cytochrome P450 and Glutathione-S-transferases. Log2 fold change values of the DEGs were imported into MapMan. Red and blue bins represent up-regulation and down-regulation as shown by the scale. (B) Significantly enriched pathways (qvalue< 0.05) for +Fe –P (P-deficiency) and –Fe –P (dual) deficiency. X-axis depicts the rich-factor, i.e., the ratio of perturbed genes in a pathway w.r.t. the total number of genes involved in the respective pathway, y-axis represents the enriched pathway names, bubble sizes depict the number of genes altered in respective pathways, and increasing intensity of blue color represents increasing significance (decreasing q-value).

Figure 6: Overview of the changes in metabolome in roots of wheat seedlings subjected to different growth regimes of Fe and P. (A) Heatmap distribution of the different metabolome (GC-MS) analysis in the respective replicates of each conditions for of the metabolites. Individual metabolites are expressed in terms of concentrations (µg/mg, fresh weight). Data are means ±SD of n=3 experiments. Metabolites are sorted according to their classes specifically, Sugars, general acids, amino acids, sugar conjugates, fatty acids and polyols. (B) Quantitative plot for the metabolite concentrations (µg/mg FW) for response specific to –Fe –P and response common in –Fe and –Fe–P. Different symbols indicate significant differences between the conditions as determined by Fisher's LSD ($p < 0.05$). +Fe +P, control; -Fe +P, Fe deficiency; +Fe –P, P deficiency; –Fe –P, Fe and P deficiency. 'a' represent significant difference against control, '#' represent significant difference against Fe deficiency and '@' represent significant difference against P deficiency. Red and green bins represent up-regulation and down-regulation with Log2 fold change values as shown by the scale.

Figure 7: Phenotype of wheat grown under different Fe/P concentrations. (A) Phenotypic representation of wheat plants subjected to multiple treatments. (B) Spike length for the respective treatments (n=5). (C) Phenotypic characteristics of different tissue of the spike (glumes, rachis and awn).

LEGEND FOR SUPPLEMENTARY DATA

Figure S1: Expression correlation within replicates and across distinct conditions from RNAseq data. A) Principal component analysis (PCA) and B) Cluster heatmap analysis of genes across different deficiency conditions (+Fe-P, –Fe+P and –Fe–P) and control (+Fe+P) for a period of 20 days in wheat roots. Genes with highest variation across these four

conditions were used for generating the heatmap using pheatmap package. The change from blue to red color in the color scale depicts increasing gene expression.

Figure S2: MapMan based functional enrichment analysis. A) Hormone biosynthesis and regulation related perturbed genes in -P (left pane) and -Fe-P (right pane) represented as bins for the respective hormones. B) Secondary metabolism related genes altered in –Fe–P condition. Log2FC values for the respective conditions w.r.t. control was used as input for MapMan, Red and blue colored bins represent up and downregulation of genes, as depicted by the scale.

Figure S3: qRT-PCR analysis of genes involved in Fe uptake/mobilization. Total of 2 µg of RNA was used for cDNA synthesis and qRT-PCR was performed using gene specific primers (Table S1). C_t values were normalized against wheat *ARF1* as an internal control.

Figure S4: MapMan metabolism overview for the DEGs in P and Fe deficiency**.** Metabolism overview demonstrating differentially expressed transcripts involved in different functional categories, under A) –P and B) –Fe–P deficiency samples w.r.t. control wheat roots. Log2FC values for the respective conditions w.r.t. control was used as input for MapMan, red and blue colored bins represent up and downregulation of genes.

Figure S5: MapMan visualization depicting the differentially expressed transcription factors families (TFs) for –P (top) and –Fe-P (bottom) conditions w.r.t. Control wheat roots. The red and blue coloured bins represent up and down-regulated transcripts. Numbers in the scale represent fold changes in expression levels expressed as Log2.

Table S1: Primers used in the current study.

Table S2: DEGs in response to Fe and P deficiency in wheat roots. List of upregulated genes and downregulated genes (multiple sheets) in respective conditions. Tables enlists genes perturbed during –P (upregulated and downregulated) and –Fe–P (upregulated and down regulated) with reference to the control samples. Our older RNAseq (Kaur et. al., 2019, BioProjectID-PRJNA529036) analysis was also repeated using Kallisto-DESeq2 pipeline, and thus -Fe (up-regulated and downregulated) perturbed genes are also listed in different sheets. DEGs were annotated with information like gene description, rice ortholog, ortholog based gene definition, KEGG Orthology, Pathways and Pfam domains, which were obtained through KOBAS 3.0 stand-alone tool, using Oryza sativa RAP-DB as reference and also using wheat RefSeq v1.1.

Table S3: Unique genes within DEGs in response to Fe and/or P deficiencyw.r.t. control in wheat roots. List of unique DEGs expressed during each respective condition, –P, –Fe and –Fe–P (upregulated and down regulated).

Table S4: Common genes among the DEGs in response to Fe and/or P deficiency w.r.t. control in wheat roots, as displayed in the Venn diagram. List of common genes regulated by –P and –Fe–P (Sheet1), –Fe and –Fe–P (Sheet2), –Fe and –P (Sheet3). Genes regulated commonly either in same or opposite direction have been included. (NC: No significant change in expression)

Table S5: List of DEGs encoding for different transcription factors those are differentially up- and downregulated. MapMan was used to identify TFs and categorize them into TF families. Table gives logFC value for deficiency vs control under –P, -Fe and –Fe–P conditions. A gradient of red and green is used for upregulated and downregulated TFs respectively.

Table S6: List of Auxin homeostasis related genes. Genes involved in Auxin biosynthesis were shortlisted using orthologs from rice obtained using KOBAS annotation tool, while other genes involved in degradation, signal transduction and auxin responsive genes were identified using MapMan.

Table S7: List of Phosphate deficiency responsive and Fe stress responsive genes. Genes central to the uptake, transport and regulation for P and Fe under the respective stresses were shortlisted.

Table S8: Common and contrasting genes specific for –P and –Fe–P. Lists for 39 genes upregulated in both –P and –Fe–P; 96 genes downregulated in both –P and –Fe–P; 146 genes that are oppositely regulated in –P and –Fe–P.

Table S9: Common and contrasting genes specific for -Fe and -Fe-P. Lists Fe altered genes that were still differentially responsive in additional absence of P, either showing the same (410 genes; 356 upregulated in both conditions, 54 downregulated in both) or contrasting pattern of expression (200 genes). Also listed are 84 genes commonly regulated in all 3 conditions.

Table S10: GC-MS analysis of wheat roots subjected to different regimes of Fe and P. Each metabolite is represented with concentrations in three independent replicate manners. For concentration calculation, individual metabolite area was normalized to sample weight and area of internal control (sorbitol). Metabolites with no detectable area in any of the conditions were considered to be the metabolite with minimum area. Delta method approximation was used to calculate standard errors (se) of log-ratio, se log-ratio = 1/ln 2√[(SET /T)2 + (SEC

/C)2], where SET and SEC are standard errors of average +Fe -P/-P +Fe/-Fe -P and +Fe +P metabolite abundances, respectively. Metabolites with significant (p-value <0.05) differential abundance were plotted.

Table S11: Percentage distribution of frequent putative cis-regulatory elements (freq-pCREs) analysed in RNASeq data. DEGs from the three deficiency conditions were selected, their promoters were searched for the presence of the 115 freq-pCREs enriched in Fe GS clusters (Schwarz et al., 2020). Percentage distribution was also analysed for FSR and PSR genes. For control sample, three sets of 100 genes with no DE under -Fe condition were randomly selected and analyzed. TF family for respective motifs were obtained from Schwarz et al., 2020.

Table S12: Percentage distribution of PHR1 binding site (P1BS) motifs in the promoter region of transcripts DE in RNASeq data and specifically in the genes involved in FSR, PSR genes (Sheet 1). PSR and FSR genes followed by the number of P1BS motifs found in each gene's promoter region (Sheet 2 and 3).

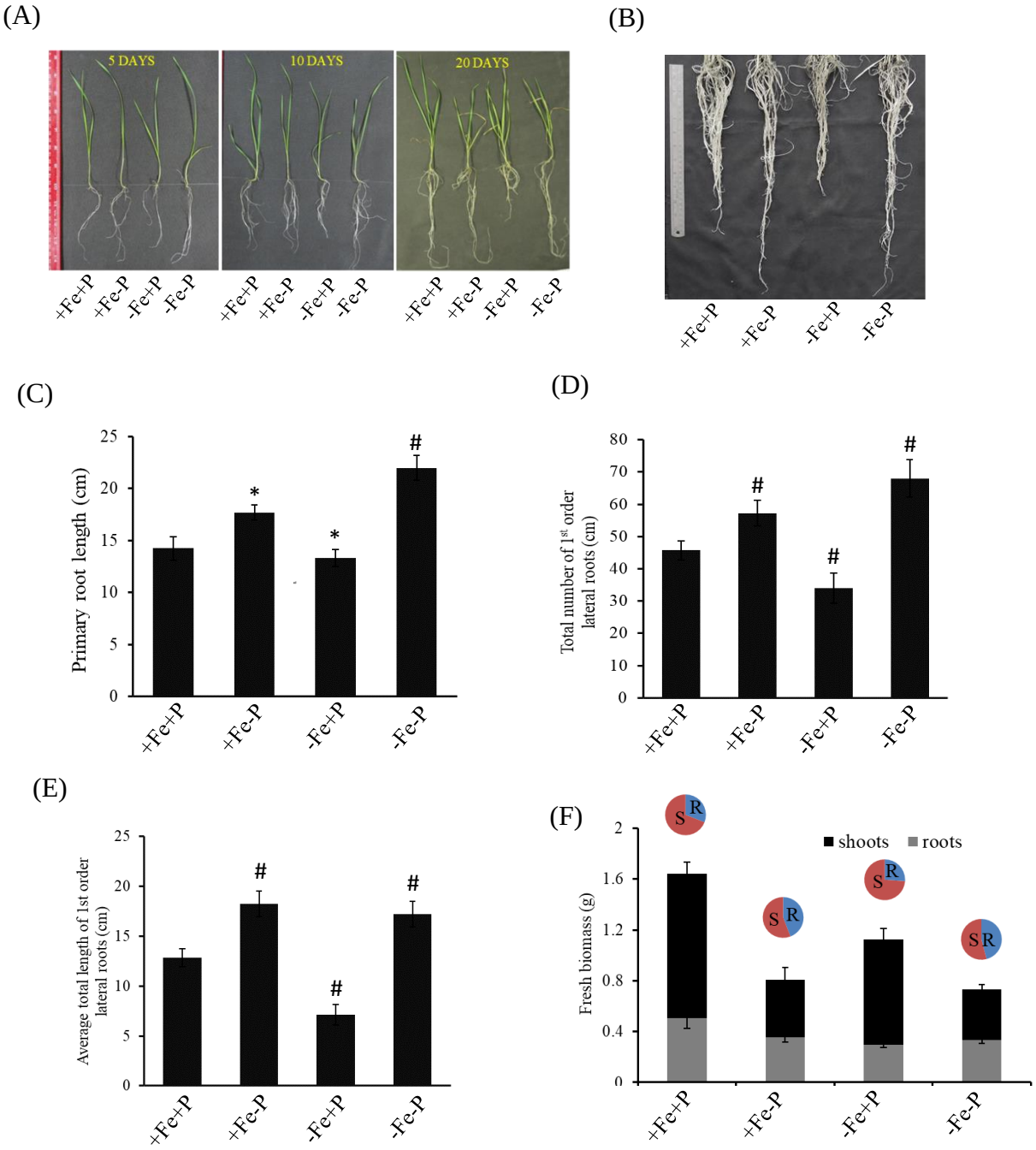
(A)
5 DAYS
10 DAYS
20 DAYS
+Fe+P
+Fe-P
-Fe+P
-Fe-P
(B)
+Fe+P
+Fe-P
-Fe+P
-Fe-P
(C)
Primary root length (cm)
25
20
15
10
5
0
*
*
#
+Fe+P
+Fe-P
-Fe+P
-Fe-P
(D)
Total number of 1st order lateral roots (cm)
80
70
60
50
40
30
20
10
0
#
#
#
+Fe+P
+Fe-P
-Fe+P
-Fe-P
(E)
Average total length of 1st order lateral roots (cm)
25
20
15
10
5
0
#
#
#
+Fe+P
+Fe-P
-Fe+P
-Fe-P
(F)
Fresh biomass (g)
2
1.6
1.2
0.8
0.4
0
shoots
roots
S
R
+Fe+P
+Fe-P
-Fe+P
-Fe-P

Figure 1

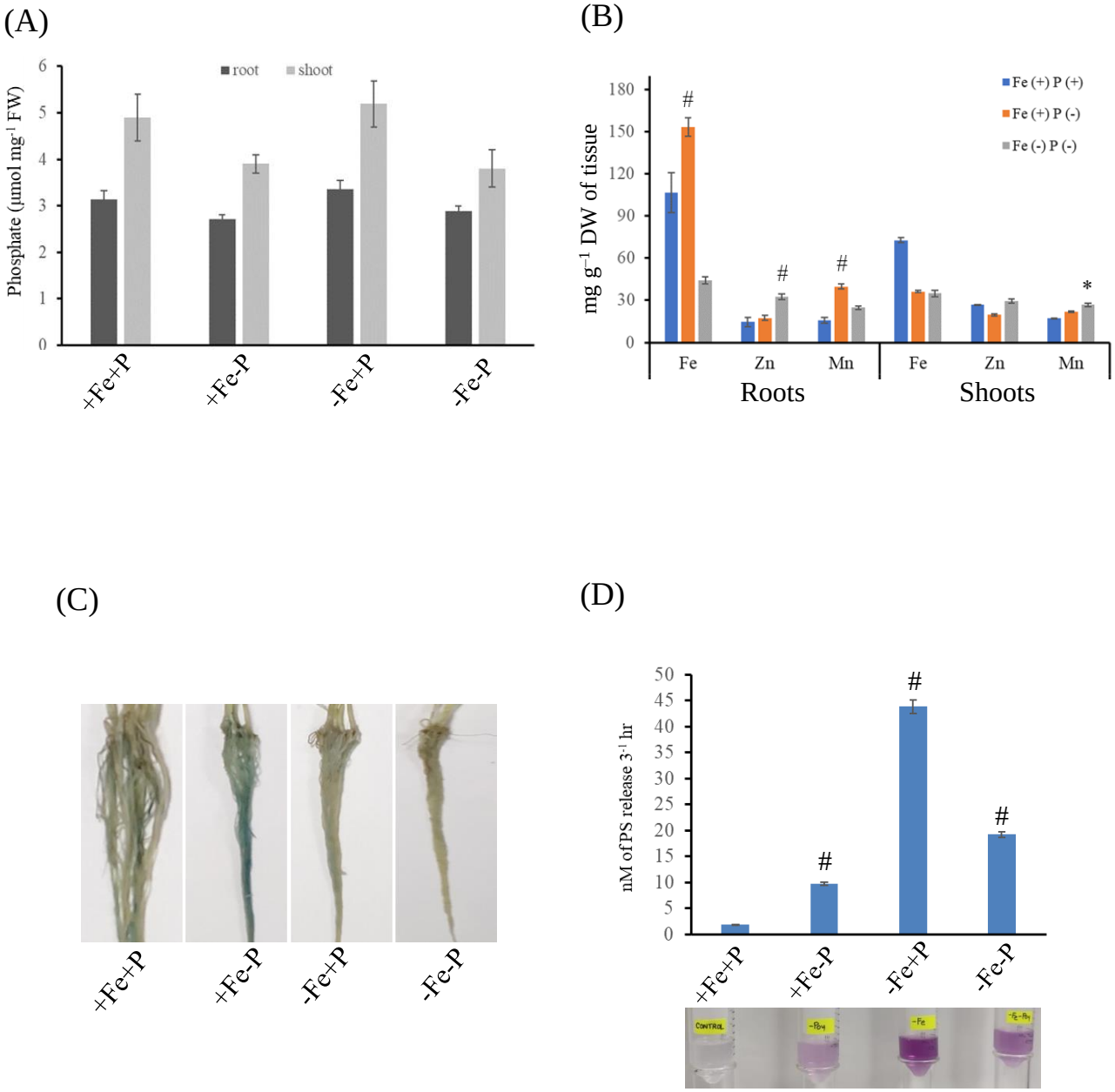
(A)
Phosphate (µmol mg-1 FW)
root
shoot
+Fe+P
+Fe-P
-Fe+P
-Fe-P
(B)
mg g-1 DW of tissue
Fe (+) P (+)
Fe (+) P (-)
Fe (-) P (-)
Fe
Zn
Mn
Roots
Shoots
(C)
+Fe+P
+Fe-P
-Fe+P
-Fe-P
(D)
nM of PS release 3-1 hr
+Fe+P
+Fe-P
-Fe+P
-Fe-P

Figure 2

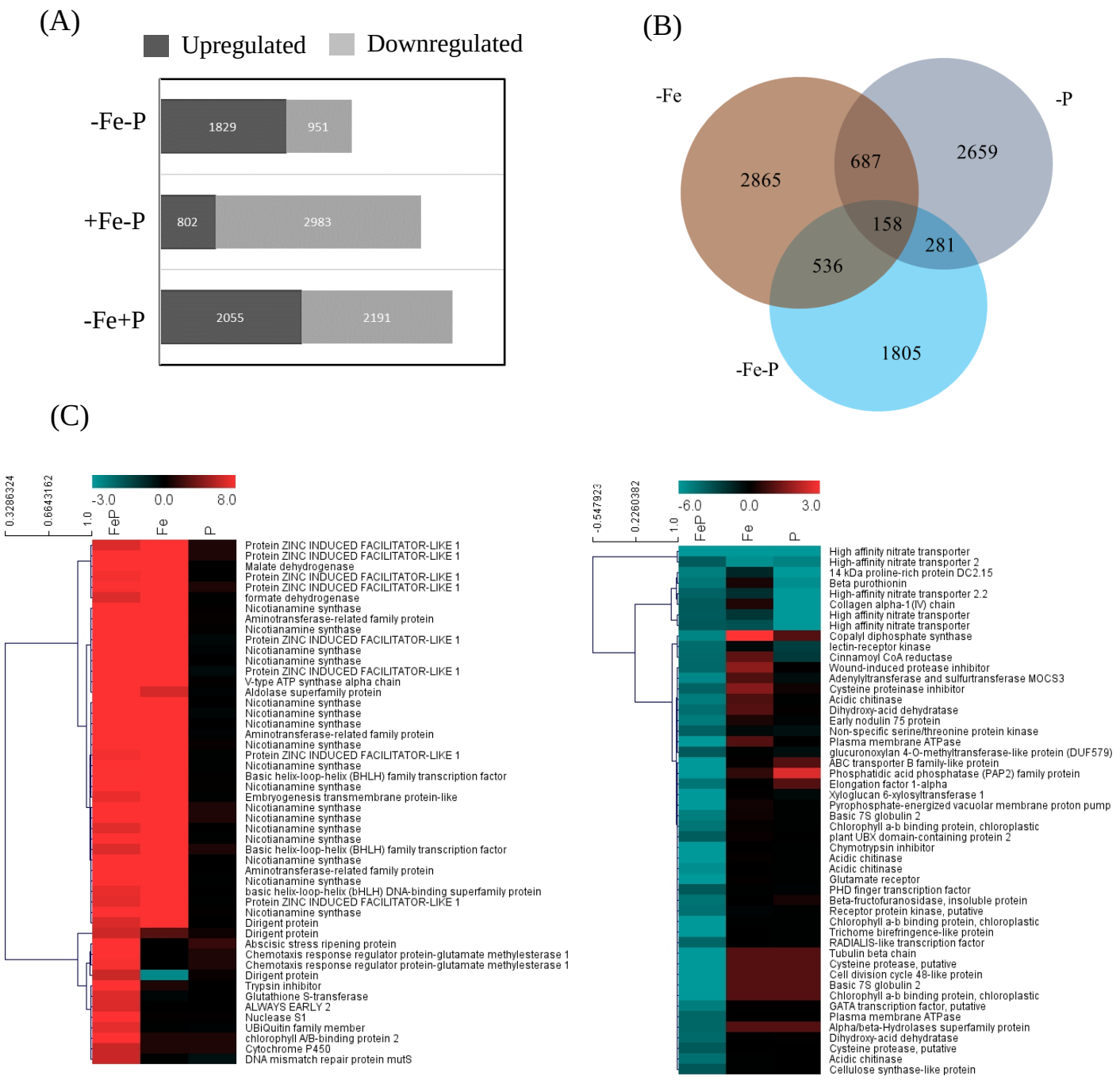
(A)
Upregulated
Downregulated
-Fe-P
1829
951
+Fe-P
802
2983
-Fe+P
2055
2191
(B)
-Fe
-P
-Fe-P
2865
687
2659
158
281
536
1805
(C)
0.3288324
0.6643162
1.0
-3.0
0.0
8.0
FeP
Fe
P
Protein ZINC INDUCED FACILITATOR-LIKE 1
Protein ZINC INDUCED FACILITATOR-LIKE 1
Malate dehydrogenase
Protein ZINC INDUCED FACILITATOR-LIKE 1
Protein ZINC INDUCED FACILITATOR-LIKE 1
formate dehydrogenase
Nicotianamine synthase
Aminotransferase-related family protein
Nicotianamine synthase
Protein ZINC INDUCED FACILITATOR-LIKE 1
Nicotianamine synthase
Nicotianamine synthase
Protein ZINC INDUCED FACILITATOR-LIKE 1
V-type ATP synthase alpha chain
Aldolase superfamily protein
Nicotianamine synthase
Nicotianamine synthase
Nicotianamine synthase
Aminotransferase-related family protein
Nicotianamine synthase
Protein ZINC INDUCED FACILITATOR-LIKE 1
Nicotianamine synthase
Basic helix-loop-helix (BHLH) family transcription factor
Nicotianamine synthase
Embryogenesis transmembrane protein-like
Nicotianamine synthase
Nicotianamine synthase
Nicotianamine synthase
Nicotianamine synthase
Basic helix-loop-helix (BHLH) family transcription factor
Nicotianamine synthase
Aminotransferase-related family protein
Nicotianamine synthase
basic helix-loop-helix (bHLH) DNA-binding superfamily protein
Protein ZINC INDUCED FACILITATOR-LIKE 1
Nicotianamine synthase
Dirigent protein
Dirigent protein
Abscisic stress ripening protein
Chemotaxis response regulator protein-glutamate methylesterase 1
Chemotaxis response regulator protein-glutamate methylesterase 1
Dirigent protein
Trypsin inhibitor
Glutathione S-transferase
ALWAYS EARLY 2
Nuclease S1
UBiQuitin family member
chlorophyll A/B-binding protein 2
Cytochrome P450
DNA mismatch repair protein mutS
-0.547923
0.2260382
1.0
-6.0
0.0
3.0
FeP
Fe
P
High affinity nitrate transporter
High-affinity nitrate transporter 2
14 kDa proline-rich protein DC2.15
Beta purothionin
High-affinity nitrate transporter 2.2
Collagen alpha-1(IV) chain
High affinity nitrate transporter
High affinity nitrate transporter
Copalyl diphosphate synthase
lectin-receptor kinase
Cinnamoyl CoA reductase
Wound-induced protease inhibitor
Adenylyltransferase and sulfurtransferase MOCS3
Cysteine proteinase inhibitor
Acidic chitinase
Dihydroxy-acid dehydratase
Early nodulin 75 protein
Non-specific serine/threonine protein kinase
Plasma membrane ATPase
glucuronoxylan 4-O-methyltransferase-like protein (DUF579)
ABC transporter B family-like protein
Phosphatidic acid phosphatase (PAP2) family protein
Elongation factor 1-alpha
Xyloglucan 6-xylosyltransferase 1
Pyrophosphate-energized vacuolar membrane proton pump
Basic 7S globulin 2
Chlorophyll a-b binding protein, chloroplastic
plant UBX domain-containing protein 2
Chymotrypsin inhibitor
Acidic chitinase
Acidic chitinase
Glutamate receptor
PHD finger transcription factor
Beta-fructofuranosidase, insoluble protein
Receptor protein kinase, putative
Chlorophyll a-b binding protein, chloroplastic
Trichome birefringence-like protein
RADIALIS-like transcription factor
Tubulin beta chain
Cysteine protease, putative
Cell division cycle 48-like protein
Basic 7S globulin 2
Chlorophyll a-b binding protein, chloroplastic
GATA transcription factor, putative
Plasma membrane ATPase
Alpha/beta-Hydrolases superfamily protein
Dihydroxy-acid dehydratase
Cysteine protease, putative
Acidic chitinase
Cellulose synthase-like protein

Figure 3

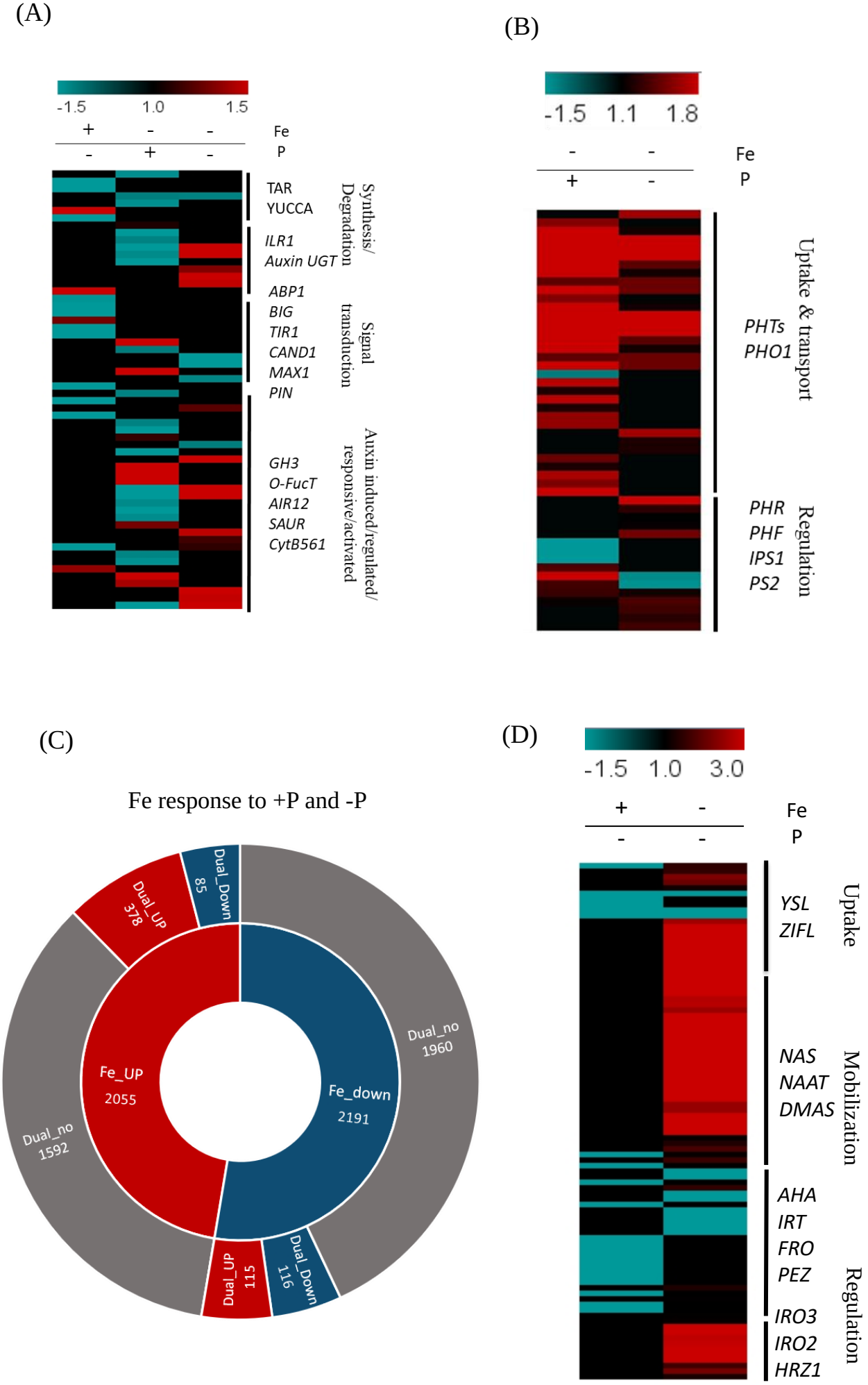
(A)
-1.5
1.0
1.5
Fe
P
TAR
YUCCA
ILR1
Auxin UGT
ABP1
BIG
TIR1
CAND1
MAX1
PIN
GH3
O-FucT
AIR12
SAUR
CytB561
Synthesis/ Degradation
Signal transduction
Auxin induced/regulated/ responsive/activated
(B)
-1.5
1.1
1.8
Fe
P
PHTs
PHO1
PHR
PHF
IPS1
PS2
Uptake & transport
Regulation
(C)
Fe response to +P and -P
Fe_UP
2055
Fe_down
2191
Dual_no
1592
Dual_no
1960
Dual_UP
378
Dual_Down
85
Dual_UP
115
Dual_Down
116
(D)
-1.5
1.0
3.0
Fe
P
YSL
ZIFL
NAS
NAAT
DMAS
AHA
IRT
FRO
PEZ
IRO3
IRO2
HRZ1
Uptake
Mobilization
Regulation

Figure 4

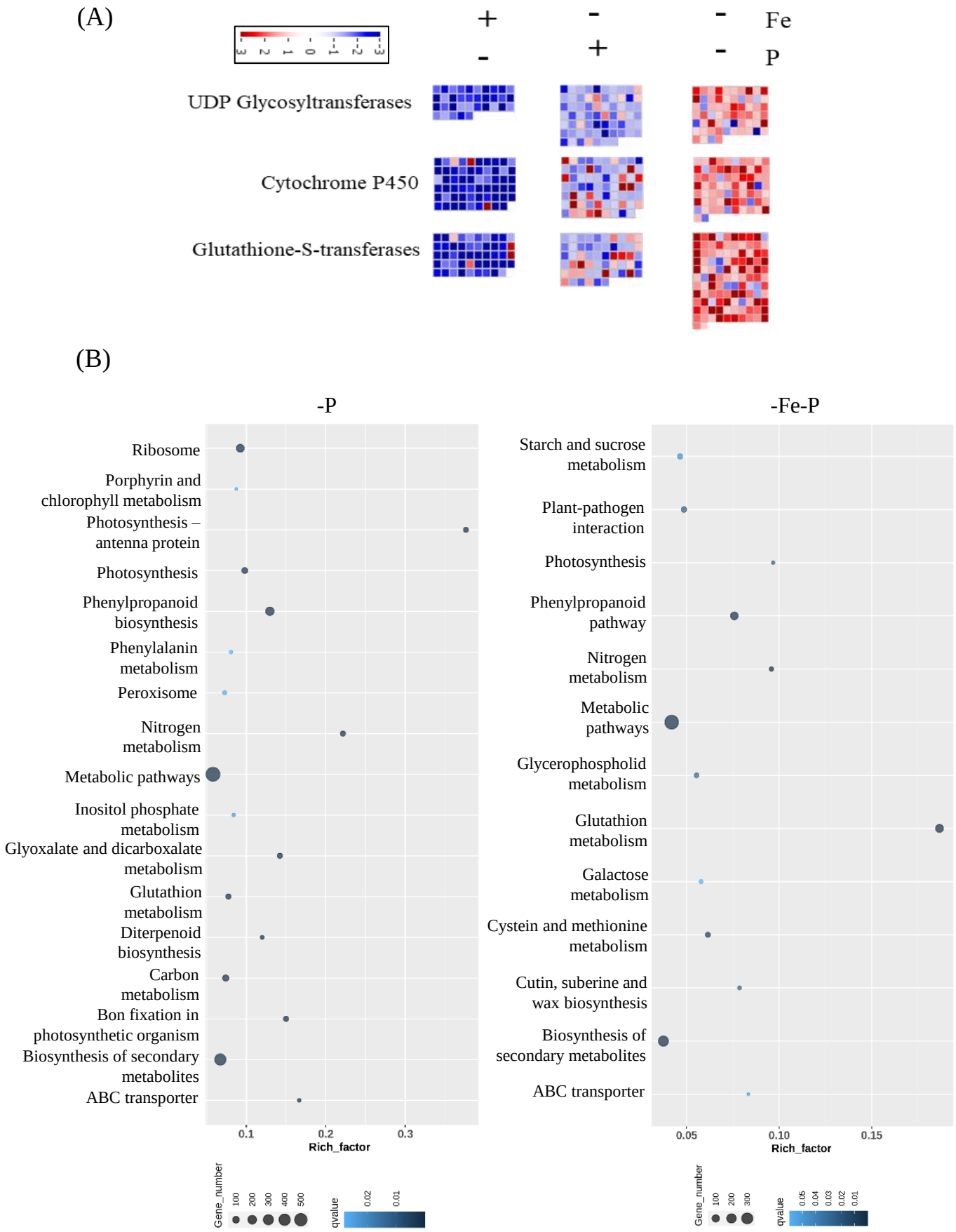
(A)
+ - - Fe
- + - P
UDP Glycosyltransferases
Cytochrome P450
Glutathione-S-transferases
(B)
-P
Ribosome
Porphyrin and chlorophyll metabolism
Photosynthesis – antenna protein
Photosynthesis
Phenylpropanoid biosynthesis
Phenylalanin metabolism
Peroxisome
Nitrogen metabolism
Metabolic pathways
Inositol phosphate metabolism
Glyoxalate and dicarboxalate metabolism
Glutathion metabolism
Diterpenoid biosynthesis
Carbon metabolism
Bon fixation in photosynthetic organism
Biosynthesis of secondary metabolites
ABC transporter
0.1
0.2
0.3
Rich_factor
Gene_number
100
200
300
400
500
qvalue
0.02
0.01
-Fe-P
Starch and sucrose metabolism
Plant-pathogen interaction
Photosynthesis
Phenylpropanoid pathway
Nitrogen metabolism
Metabolic pathways
Glycerophospholid metabolism
Glutathion metabolism
Galactose metabolism
Cystein and methionine metabolism
Cutin, suberine and wax biosynthesis
Biosynthesis of secondary metabolites
ABC transporter
0.05
0.10
0.15
Rich_factor
Gene_number
100
200
300
qvalue
0.05
0.04
0.03
0.02
0.01

Figure 5

(A)

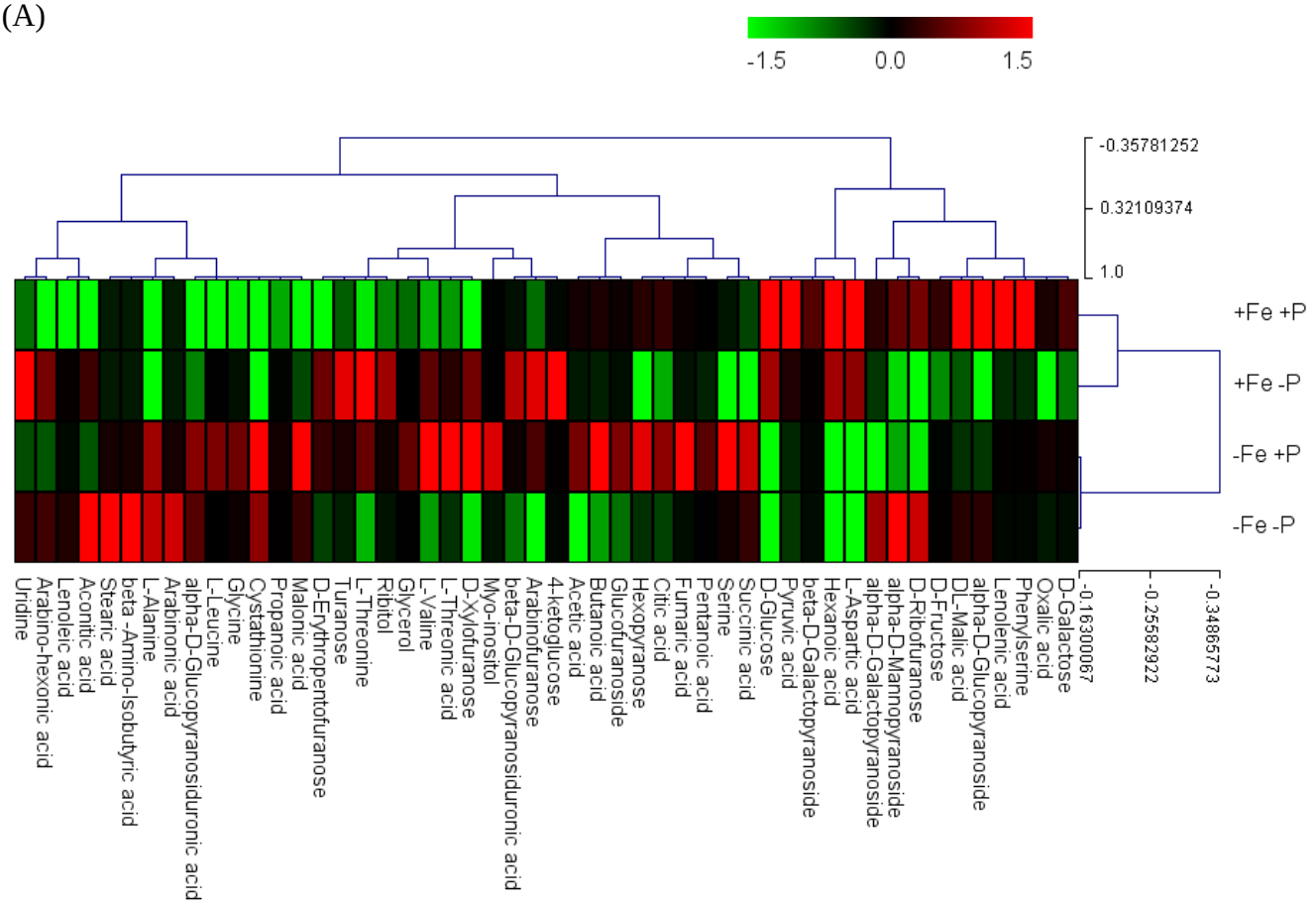
-1.5
0.0
1.5
-0.35781252
0.32109374
1.0
+Fe +P
+Fe -P
-Fe +P
-Fe -P
-0.16300067
-0.25582922
-0.34865773
D-Galactose
Oxalic acid
Phenylserine
Lenolenic acid
alpha-D-Glucopyranoside
DL-Malic acid
D-Fructose
D-Ribofuranose
alpha-D-Mannopyranoside
alpha-D-Galactopyranoside
L-Aspartic acid
Hexanoic acid
beta-D-Galactopyranoside
Pyruvic acid
D-Glucose
Succinic acid
Serine
Pentanoic acid
Fumaric acid
Citric acid
Hexopyranose
Glucofuranoside
Butanoic acid
Acetic acid
4-ketoglucose
Arabinofuranose
beta-D-Glucopyranosiduronic acid
Myo-inositol
D-Xylofuranose
L-Threonic acid
L-Valine
Glycerol
Ribitol
L-Threonine
Turanose
D-Erythropentofuranose
Malonic acid
Propanoic acid
Cystathionine
Glycine
L-Leucine
alpha-D-Glucopyranosiduronic acid
Arabinonic acid
L-Alanine
beta -Amino-Isobutyric acid
Stearic acid
Aconitic acid
Lenoleic acid
Arabino-hexonic acid
Uridine

(B)

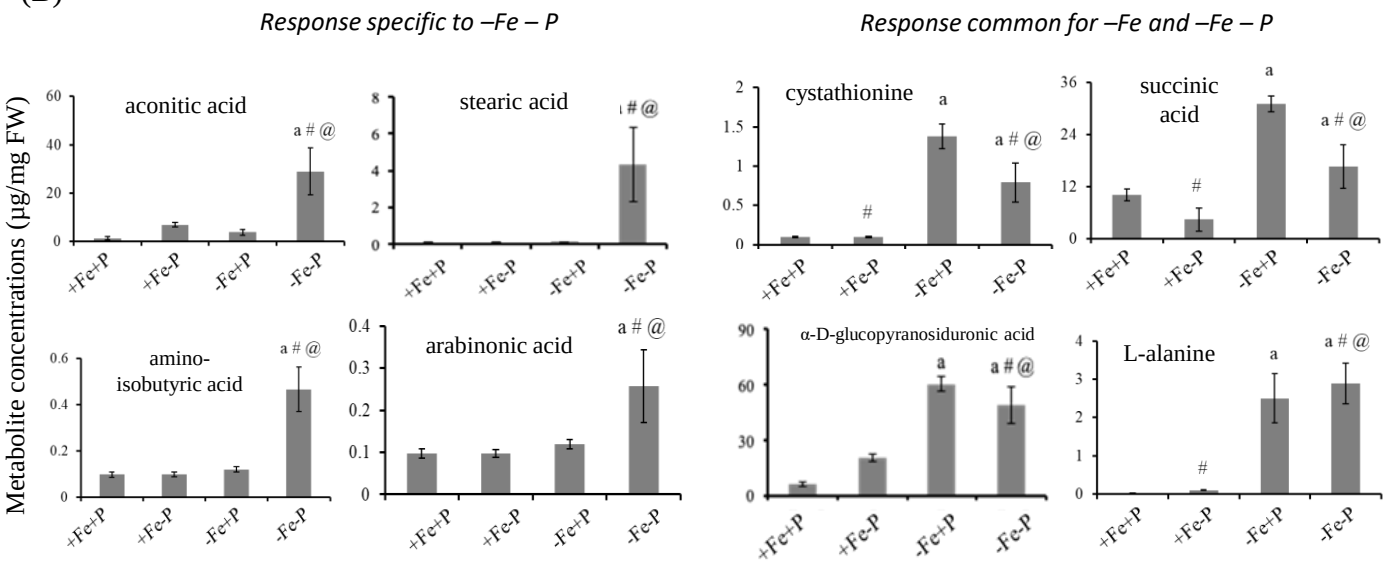
Response specific to –Fe – P
Response common for –Fe and –Fe – P
Metabolite concentrations (µg/mg FW)
aconitic acid
stearic acid
cystathionine
succinic acid
amino-isobutyric acid
arabinonic acid
α-D-glucopyranosiduronic acid
L-alanine
+Fe+P
+Fe-P
-Fe+P
-Fe-P
a # @
a
#

Figure 6

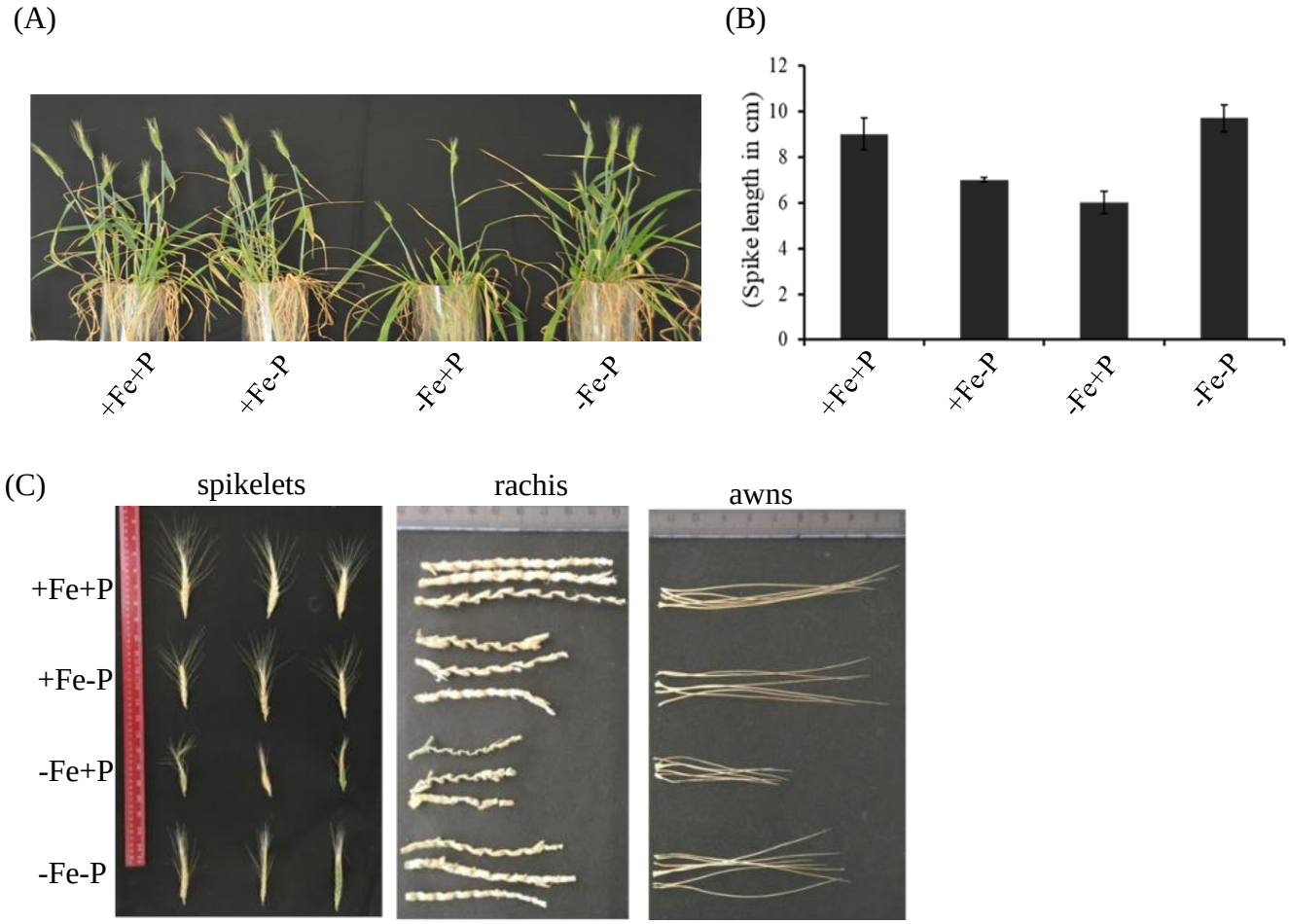
(A)
+Fe+P
+Fe-P
-Fe+P
-Fe-P
(B)
(Spike length in cm)
0
2
4
6
8
10
12
+Fe+P
+Fe-P
-Fe+P
-Fe-P
(C)
spikelets
rachis
awns
+Fe+P
+Fe-P
-Fe+P
-Fe-P

Figure 7